Adaptive resilience strategies for supply chain networks against disruptions

Hart Nibbrig, Maurice; Sharif Azadeh, Shadi; Maknoon, M. Y.

DOI
10.1016/j.tre.2025.104172

Publication date
2025

Document Version
Final published version

Published in
Transportation Research Part E: Logistics and Transportation Review

Citation (APA)
Hart Nibbrig, M., Sharif Azadeh, S., & Maknoon, M. Y. (2025). Adaptive resilience strategies for supply chain networks against disruptions. *Transportation Research Part E: Logistics and Transportation Review*, *200*, Article 104172. https://doi.org/10.1016/j.tre.2025.104172

Transportation Research Part E 200 (2025) 104172

Contents lists available at ScienceDirect

Transportation Research Part E

journal homepage: www.elsevier.com/locate/tre

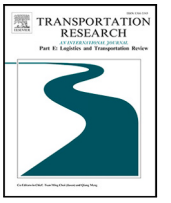

Adaptive resilience strategies for supply chain networks against disruptions

Maurice Hart Nibbrig [a], Shadi Sharif Azadeh [b], M.Y. Maknoon [a,*]

[a] Faculty of Technology, Policy, and Management, Delft University of Technology, Delft, Netherlands
[b] Faculty of Civil Engineering and Geosciences, Delft University of Technology, Delft, Netherlands

ARTICLE INFO

Keywords:
Supply chain resilience
Climate-related disruptions
Mixed-integer optimization
Adaptive reinforcement
Resilience evaluation

ABSTRACT

Supply chain networks face the critical challenge of enhancing resilience to disruptions while controlling the costs associated with resilience improvements. In this paper, we introduce an adaptive resilience improvement framework designed to sustain material flow by responding dynamically to emerging network vulnerabilities. Our framework centers on the production chain as a core element in resilience planning, integrating vulnerability assessment and reinforcement strategies through a tri-level optimization model. This model adapts to the network's changing conditions by (i) incorporating disruption scenario generation as an integral part of the decision-making process, allowing for the dynamic identification of vulnerabilities, and (ii) optimizing reinforcement strategies in response to them. We demonstrate the framework's effectiveness through two distinct case studies: a steel supply chain, where production flexibility improves resilience by 30%, and a pharmaceutical supply chain affected by climate-related disruptions. Our computational results confirm the scalability and effectiveness of this approach in strengthening network-wide resilience as vulnerabilities evolve.

1. Introduction

This paper introduces an adaptive resilience improvement framework for enhancing the resilience of supply chain networks, with a focus on sustaining material flows during disruptions. As supply chains expand across regions and industries, their increasing scale and interdependence expose them to a broader range of disruptions. Although localized vulnerabilities can often be identified, a more complex challenge lies in assessing how disruptions at one point in the network can lead to significant supply shortfalls at other points.

Network resilience in supply chains involves long-term strategies to strengthen the network's capacity to withstand and absorb disruptions (Wieland and Durach, 2021). Enhancing network resilience relies on three interrelated components: scenario mapping to outline potential chains of disruption, assessment to measure the impact of each scenario on the supply chain operation, and targeted reinforcement strategies for improvement.

Research on supply chain resilience primarily falls into two groups. The first group focuses on assessing supply chain networks' vulnerability to disruptions (see, for example, Kim et al., 2011; Dixit et al., 2020). The second group, in contrast, focuses on determining cost-effective reinforcement strategies for supply chain networks (see, for example, Aldrighetti et al., 2023; Alikhani et al., 2023; Goldbeck et al., 2020). Key strategies include redundancy — such as establishing alternative suppliers or increasing

* Corresponding author.
E-mail addresses: m.v.r.hartnibbrig@student.tudelft.nl (M. Hart Nibbrig), s.sharifazadeh@tudelft.nl (S. Sharif Azadeh), M.Y.Maknoon@tudelft.nl (M.Y. Maknoon).

https://doi.org/10.1016/j.tre.2025.104172
Received 18 November 2024; Received in revised form 25 April 2025; Accepted 28 April 2025
Available online 17 May 2025

reserve stock levels — and flexibility, which enables adjustments in production processes or redirecting flows through alternate logistics paths to maintain continuity (Tang, 2006).

A primary objective in reinforcing network resilience is to achieve maximum network-wide resilience with minimal cost. Studies on supply chain resilience typically rely on a set of predefined scenarios to guide reinforcement strategies. These scenarios are identified based on the anticipated impact of specific disruptions on the existing network structure. However, reinforcement strategies based on predefined scenarios may not necessarily improve overall network resilience. When reinforcement strategies are applied, the network structure is altered. This potentially introducing new vulnerabilities with similar or even greater negative impacts. Given these limitations, effective resilience planning requires adaptable scenario generation within the decision-making process.

To address these challenges, we develop an integrated optimization framework that jointly determines vulnerability assessments and adaptive reinforcement strategies to enhance supply chain resilience. A central contribution of this work is the explicit modeling of the production chain as the structural conduit linking scenario-based vulnerability identification with strategic reinforcement planning. By endogenizing disruption scenarios within the decision process, we formulate a tri-level mixed-integer optimization model. The first level characterizes the production process and associated resource flows; the second level constructs endogenous vulnerability scenarios; and the third level selects reinforcement actions that mitigate network-wide risk exposure. To ensure computational tractability for large-scale instances, we introduce a customized decomposition framework that partitions the problem into a single-level master problem and a bilevel subproblem.

A further contribution lies in the empirical validation of both scalability and practical relevance. We demonstrate computational performance via benchmark tests that quantify the influence of key structural parameters on solution time. Practical value is illustrated through two real-world case studies. In a steel supply chain, we show that production flexibility improves delivery reliability by 30% without incurring additional reinforcement costs. In a global pharmaceutical network, the framework supports both system redesign and long-term resilience planning under climate-induced disruptions. These case studies underscore how the proposed framework can inform strategic investment in resilience for complex and evolving supply chain environments.

The structure of the paper is as follows: Section 2 reviews the existing literature on supply chain resilience. Section 3 introduces the conceptual model and its mathematical formulation. Section 4 describes the resolution strategy. Finally, Section 5 presents the computational experiments and case studies.

2. Related literature

Supply chain resilience strategies aim to mitigate vulnerabilities and maintain continuity amid disruptions by addressing resilience across three key dimensions: Organizational Resilience, Operational Resilience, and Structural Resilience. Organizational resilience focuses on relational factors that support adaptability and coordination; operational resilience emphasizes immediate decision-making for response; and structural resilience involves long-term strategies to reinforce supply chain networks. This review is structured around these dimensions. For broader discussions on supply chain resilience, see Hosseini et al. (2019), Ivanov et al. (2017), Kamalahmadi and Parast (2016), Ribeiro and Barbosa-Povoa (2018), Tukamuhabwa et al. (2015).

Organizational resilience relies on relational factors and digital tools that support adaptability and quick response to disruptions. Studies highlight the role of social capital — trust, shared goals, and communication — in strengthening resilience. For instance, Brusset and Teller (2017) demonstrate that integration (coordination across functions) and flexibility (the ability to adapt quickly) are essential for managing disruptions. Similarly, Johnson et al. (2013) and Wieland and Wallenburg (2013) find that social capital, including shared networks, enhances resilience by building trust and collaboration. Extending this concept, Saglam et al. (2022) show that communication quality, commitment, and reciprocity contribute to resilience by reinforcing trust-based relationships.

Digital tools are also crucial for resilience. Tiwari et al. (2024) show that visibility and digital technologies improve information flow and coordination, enabling healthcare supply chains to respond more effectively to disruptions. Liu et al. (2024) find that supplier and customer integration, supported by big data analytics, enhances adaptability and stability. Supplier integration promotes rapid adaptation, while customer integration aids continuity through real-time data. Similarly, Blackhurst et al. (2011) and Boone et al. (2013) demonstrate that real-time monitoring and adaptive inventory management allow for early risk detection and swift response. Finally, Brandon-Jones et al. (2015) find that slack resources and visibility help absorb shocks and maintain performance during disruptions.

Operational resilience is an organization's capacity to respond to disruptions, manage risks, and prevent cascading failures. A key challenge is managing ripple effects, where disruptions spread across interconnected components. Dolgui et al. (2018) and Ivanov et al. (2014) suggest that combining redundancy with material flow reconfiguration helps contain these effects, while Han and Shin (2016) propose using structural metrics to monitor disruption spread. Building on these concepts, Pavlov et al. (2017) recommend a hybrid approach integrating proactive and reactive measures for enhanced resilience. Recent extensions address risk-averse decision-making and disruption recovery across varied contexts. Sawik and Sawik (2024) introduce a viability-preserving model under disruption propagation; Li and Yuan (2024) develop profitability-aware recovery strategies for joint supply–demand disruptions; and Roi et al. (2023) propose an adaptive framework under stochastic conditions. In a distinct application, Sawik (2023) examine supply chain optimization in the context of space mission risk and sustainability. Meanwhile, consumer-centric resilience efforts are emerging, as in Sawik (2024), which explores last-mile delivery robustness through smart lockers and crowdshipping.

Effective disruption management also aligns internal capabilities with network resources. For instance, Li et al. (2023) find that matching internal competencies, like product diversity, with network features enhances resilience. Studies during the COVID-19 pandemic, such as Ramani et al. (2022), further illustrate how network vulnerabilities affect supply chains. To address these

Table 1
Positioning of the current study within the resilience literature.

Study	Uncertainty Source	Type Type	Scenario Generation	Approach (SO/RO/AO)	Resilience Strategy
Yılmaz et al. (2023)	Demand	Unknowable	Exogenous	SO + RO	Redundancy
Yılmaz et al. (2021)	Supply	Knowable	Exogenous	SO	Redundancy
Özçelik et al. (2021)	Supply	Knowable	Exogenous	RO	Redundancy
Hasani and Khosrojerdi (2016)	Demand	Knowable	Exogenous	RO	Redundancy, Flexibility
Aldrighetti et al. (2023)	Supply, Demand	Knowable	Exogenous	SO	Redundancy
Goldbeck et al. (2020)	Supply	Knowable	Exogenous	SO (multi-stage)	Redundancy
This study	Supply	Unknowable	Endogenous	AO	Redundancy, Flexibility

issues, Hosseini and Ivanov (2022) and Liu et al. (2023) recommend assessing supplier vulnerabilities and leveraging network support.

Redundancy and flexibility are key resilience strategies. Redundancy provides buffers, such as inventory and diversified suppliers, while flexibility supports adaptation through production adjustments. Ishfaq (2012) and Wang et al. (2016) show that flexible transportation and rerouting can help manage disruptions, though rerouting may sometimes reduce robustness (Adenso-Díaz et al., 2018). Beyond transportation, resilience can be enhanced through buffer stock, alternative routes, and multi-echelon networks (Carvalho et al., 2012; Cardoso et al., 2015). Recent studies have extended the analysis of ripple effects to reverse supply chains, employing both robust and stochastic optimization frameworks. For example, Yılmaz et al. (2021) develop a two-stage stochastic model that jointly minimizes cost and environmental impact under disruption scenarios. In a related effort, Özçelik et al. (2021) formulate a robust optimization approach to enhance the resilience of reverse logistics networks, validated through an industrial case study.

Inventory management complements these strategies by maintaining flow during disruptions. Approaches such as Risk Mitigation Inventory (RMI), dual sourcing, and agile responses position inventory effectively and ensure continuity (Lücker and Seifert, 2017; Gao et al., 2019). Extending this, Sawik (2022) show that pre-positioned RMI and backup suppliers improve service levels during multi-regional disruptions like COVID-19.

Unlike organizational and operational resilience, which focus on responding to disruptions as they arise, structural resilience adopts a proactive approach, aiming to design robust network configurations capable of withstanding disruptions. This requires identifying network features that help maintain material flow and absorb shocks before disruptions occur.

Several studies assess structural resilience by examining static network properties that influence disruption propagation. For example, Kim et al. (2011) highlight that network features like centrality and density support resilience by sustaining operations, whereas Bode and Wagner (2015) find that high structural complexity can increase disruption frequency. Studies like Hearnshaw and Wilson (2013) and Kim et al. (2015) argue that scale-free networks with centralized hubs offer better resistance to cascading failures, though they depend heavily on hub robustness.

Moving beyond static topologies, research has expanded to balance vulnerabilities and capabilities within networks. Pettit et al. (2013) introduce a framework for pairing risks with mitigating capabilities, while Raaymann and Spinler (2024) show that tier-specific resilience strategies are essential in complex supply chains, such as automotive. Adaptive assessment methods also emerge in recent studies: Burgos and Ivanov (2021) use digital twins to evaluate resilience in food retail during COVID-19, and Dixit et al. (2020) find that networks with lower density, higher connectivity, and larger size better withstand cascading disruptions.

While these assessment studies focus on identifying weak points and simulating disruption impacts, they often overlook strategies to actively fortify the network. Addressing this gap, studies like Yılmaz et al. (2023) and Goldbeck et al. (2020) propose reinforcement strategies under demand-side and supply-side uncertainties, respectively. These include redundancy investments, decentralized configurations, and scenario-based planning for resilience. Expanding to both supply and demand disruptions, Hasani and Khosrojerdi (2016) and Aldrighetti et al. (2023) develop models that balance preparedness with recovery, integrating strategies like facility dispersion, safety stock, and multi-sourcing.

Table 1 presents a comparative synthesis of the most relevant contributions to supply chain resilience, structured around core modeling dimensions. These include the origin of uncertainty — whether disruptions arise from supply-side failures (e.g., facility outages) or demand-side volatility — and the nature of uncertainty, categorized as known (probabilistic), knowable (bounded but partially characterized), or unknowable (unpredictable, high-impact events such as adversarial disruptions).

The table also distinguishes how disruption scenarios are modeled: exogenously, based on predefined data or expert input, or endogenously, as part of the optimization process. Modeling frameworks are classified as stochastic optimization (SO), robust optimization (RO), or adversarial optimization (AO), each reflecting distinct assumptions about disruption behavior and anticipation strategies. Finally, resilience mechanisms are grouped into two categories: *redundancy*, involving structural buffers such as backup capacity and inventory; and *flexibility*, defined as the system's adaptive capability through production switching or configuration reallocation.

While existing studies provide valuable insights into managing specific disruptions, targeted reinforcements alone often fall short of enhancing resilience across the entire network. This is because, in interconnected supply chains, interventions can inadvertently create new vulnerabilities, leading to a costly cycle of reassessment and reinforcement. Addressing this gap, our study introduces an integrative approach that embeds vulnerability identification and impact assessment within reinforcement strategies, enabling a more comprehensive improvement in network resilience while managing associated costs. Section 3 outlines the key components of our mathematical model.

3. Problem description

This study investigates the strategic design of a multi-stage supply chain to enhance structural resilience against worst-case disruptions under fixed budgetary constraints. Decisions on node fortification and production reconfiguration are made ex-ante, assuming full knowledge of network structure, reinforcement options, and the available resilience budget. The supply chain comprises four sequential stages: *suppliers* (S) for raw material procurement, *producers* ($\mathcal{P}$) for manufacturing and assembly, *warehouses* ($\mathcal{W}$) for distribution, and *end-users* (C) who receive final products. Commodities—represented by the set P—include raw materials, intermediates, and finished goods, flowing through these stages via a predefined bill of materials. Disruptions are modeled adversarially to simulate worst-case conditions that challenge network operability. The objective is to identify reinforcement and transformation strategies that maximize delivery performance under such stress. The decision framework comprises four core components, detailed in the following sections.

Supply Chain Operation. The supply chain operation is modeled as a multi-commodity network flow problem on a graph $G = \{V, E\}$, which integrates the production process, represented by the graph $\tilde{G}$, and the physical network, denoted by the graph $\bar{G}$. The graph $\tilde{G}$ captures the transformation of commodities through production processes as defined by Bills of Materials (BoMs). Let $p \in P$ denote a commodity from the set of commodities, and $b \in B$ represent a production step in the BoM. The production process is modeled as a directed graph $\tilde{G} = \{N, \tilde{E}\}$, where N contains the following nodes: n_p^{Source} (entry of commodity p), n_p^{Store} (storage of p), n_p^{Sink} (final delivery of p), and $n_b^{Convert}$ (conversion of inputs to outputs according to the BoM). The arcs $\tilde{E}$ represent the flows of commodities between these production stages.

The graph $\bar{G} = \{V, \bar{E}\}$ models the transportation of commodities between supply chain locations, where $V = V^S \cup V^{\mathcal{P}} \cup V^{\mathcal{W}} \cup V^C$ represents the locations of suppliers (S), producers ($\mathcal{P}$), warehouses ($\mathcal{W}$), and end-users (C), respectively. The set of arcs $\bar{E}$ denotes the available transportation links between these locations. By mapping $\tilde{G}$ onto $\bar{G}$, we form the supply chain operation graph G. Nodes from $\tilde{G}$, such as n_p^{Source}, n_p^{Store}, n_p^{Sink}, and $n_b^{Convert}$, are mapped to their corresponding physical locations (V) in $\bar{G}$. The arcs in E represent the movement of commodities between these locations, considering the available transportation modes and flows of commodities $p \in P$.

Disruption. Supply chain disruptions are defined as shocks that impair one or more components of the supply chain, such as facilities, suppliers, transportation links, or production capacities. Each node in the supply chain network is associated with a function that quantifies the risk at that node, typically measured in terms of reduced operational capacity. These risks can originate from various sources, including external factors like climate-induced events. As noted by Forster et al. (2021), climate-induced events — such as floods, storms, and heatwaves — are driven primarily by region-specific meteorological systems and geographical conditions, making them generally uncorrelated across different locations. Given this spatial and temporal independence, we assume that the occurrence of such events at geographically dispersed nodes in the supply chain can be treated as independent.

We aim to uncover critical vulnerabilities and assess the resilience of the supply chain by identifying the worst possible timing and combination of disruptions. To achieve this, we introduce the concept of a hypothetical adversary, representing strategic foresight, tasked with selecting a set of disruptions that would cause the maximum possible damage to the supply chain. This adversarial approach serves as a stress-test, simulating how strategic foresight can anticipate and prepare for the most harmful combinations of disruptions. The analysis is conducted under a budget constraint.

Recovery Period. After a disruption, the supply chain adjusts to meet demand under new operational constraints. The time required to restore functionality at different locations varies depending on factors such as the severity of the disruption, the node's role within the supply chain, and the availability of recovery resources. Our goal is to evaluate the supply chain's performance over an extended period. The recovery period is modeled as the union of intervals representing the restoration of functionality at individual components, capturing the heterogeneity in recovery across various locations.

Resilient Design and reinforcement. Resilient design, also known as reinforcement, refers to a set of actions aimed at increasing the robustness and adaptability of the supply chain. These actions can be implemented at individual nodes (e.g., suppliers, warehouses) or across the entire network. Conceptually, resilient design strategies are divided into two primary approaches: adding redundancy (e.g., increasing the number of suppliers or expanding storage capacity) and enhancing production flexibility (e.g., enabling production shifts between locations). Each resilience or reinforcement strategy incurs a specific cost, which must be managed within a predefined budget constraint.

Illustrative Example: Consider a simplified supply chain network comprising 2 suppliers (S1, S2), 3 production facilities (P1, P2, P3), 1 warehouse (W1), and 2 customers (C1, C2). Material flows for six product types ($M1$–$M6$) follow a predefined bill of materials (BoM). Fig. 1(a) shows the baseline network configuration.

Assume that the model identifies P1 as the most critical node through vulnerability assessment under a given resilience budget. To enhance network resilience, it recommends two feasible reinforcement strategies, each aligned with a different budget level:

- Strategy 1 – Production Flexibility: Under a limited budget, the model upgrades P2 to absorb part of P1's output (specifically $M5$), introducing cross-facility flexibility (Fig. 1(b)).
- Strategy 2 – Facility Expansion: With a moderately higher budget, the model adds a new production facility (P4) that receives input from both suppliers and replicates part of P1's output. This reduces reliance on P1 and improves structural robustness (Fig. 1(c)).

This example demonstrates how the model adapts to resource constraints and supports strategic trade-offs between flexibility and redundancy to strengthen operational resilience.

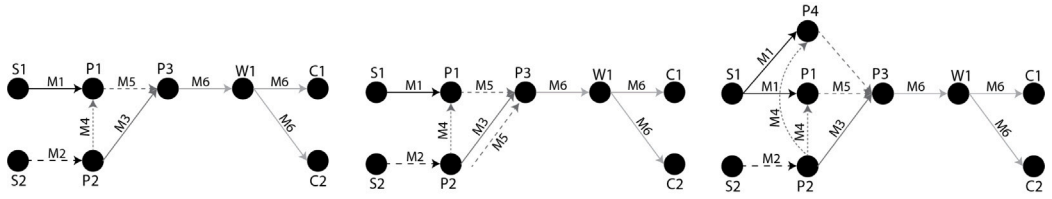

(a) Original network (b) Production flexibility strategy (c) Facility expansion strategy

Fig. 1. Illustrative example of resilient supply chain redesign: (a) original network; (b) improved via production flexibility; (c) improved via added facility.

3.1. Formulation

We model the problem as a tri-level optimization framework involving three agents: the Operator ($\mathcal{O}$), the Disruptor (i.e., Strategic foresight) ($\mathcal{D}$), and the Resilience Designer (i.e., Fortification) ($\mathcal{R}$). Each agent's objective represents a distinct decision-making process. The Operator ($\mathcal{O}$) seeks to minimize operational costs while meeting customer demand, given the current state of the system. The Disruptor (i.e., Strategic foresight) ($\mathcal{D}$) aims to maximize disruption by targeting critical nodes or links within the supply chain, constrained by a disruption budget $\beta^{\mathcal{D}}$, with the goal of increasing unmet demand. The Resilience Designer (i.e., Fortification) ($\mathcal{R}$) implements strategic interventions to minimize the impact of disruptions, subject to a resilience budget $\beta^{\mathcal{R}}$.

The tri-level optimization problem ($\mathcal{ODR}$) is formulated as follows:

$$\begin{aligned} \mathcal{ODR} \quad \min_{\boldsymbol{x}^{\boldsymbol{\mathcal{R}}}} \max_{\boldsymbol{x}^{\boldsymbol{\mathcal{D}}}} \min_{\boldsymbol{x}^{\mathcal{O}}} \quad & \Gamma^{\mathcal{O}}(\boldsymbol{x}^{\mathcal{O}}, \boldsymbol{x}^{\boldsymbol{\mathcal{D}}}, \boldsymbol{x}^{\boldsymbol{\mathcal{R}}}) \\ \text{s.t.} \quad & \boldsymbol{x}^{\mathcal{O}} \in X^{\mathcal{O}}(\boldsymbol{x}^{\boldsymbol{\mathcal{D}}}, \boldsymbol{x}^{\boldsymbol{\mathcal{R}}}), \\ & \Gamma^{\mathcal{D}}(\boldsymbol{x}^{\boldsymbol{\mathcal{D}}}) \le \beta^{\mathcal{D}}, \\ & \Gamma^{\mathcal{R}}(\boldsymbol{x}^{\boldsymbol{\mathcal{R}}}) \le \beta^{\mathcal{R}}. \end{aligned}$$

The objective function $\Gamma^{\mathcal{O}}$ represents the operator's performance cost, which is influenced by the decisions of both the disruptor ($\boldsymbol{x}^{\boldsymbol{\mathcal{D}}}$) and the resilience designer ($\boldsymbol{x}^{\boldsymbol{\mathcal{R}}}$). The operator's decision variables $\boldsymbol{x}^{\mathcal{O}}$ are constrained by the feasible operation set $X^{\mathcal{O}}$, which is shaped by both disruption and resilience strategies. The disruptor and resilience designer are each subject to their respective budget constraints, $\Gamma^{\mathcal{D}}(\boldsymbol{x}^{\boldsymbol{\mathcal{D}}}) \le \beta^{\mathcal{D}}$ for the disruptor and $\Gamma^{\mathcal{R}}(\boldsymbol{x}^{\boldsymbol{\mathcal{R}}}) \le \beta^{\mathcal{R}}$ for the resilience designer. Detailed models for the decisions of each agent are presented in the following sections.

3.2. Supply chain operation

The operator's problem is formulated as a multi-commodity network flow problem on the graph G. The vector of operational variables is given by:

$$\boldsymbol{x}^{\mathcal{O}} = \begin{bmatrix} \boldsymbol{q}^{\mathcal{S}} & \boldsymbol{q}^{\mathcal{P}} & \boldsymbol{q}^{\mathcal{W}} & \boldsymbol{q}^{\mathcal{C}} & \bar{\boldsymbol{q}}^{\mathcal{C}} & \boldsymbol{y} & \boldsymbol{z} \end{bmatrix},$$

where $\boldsymbol{q}^{\mathcal{S}}$, $\boldsymbol{q}^{\mathcal{P}}$, and $\boldsymbol{q}^{\mathcal{W}}$ represent decision variables for the quantities of commodities at suppliers ($\mathcal{S}$), producers ($\mathcal{P}$), and warehouses ($\mathcal{W}$), respectively. The variables $\boldsymbol{q}^{\mathcal{C}}$ and $\bar{\boldsymbol{q}}^{\mathcal{C}}$ denote the quantities of products delivered and not delivered to end-users ($\mathcal{C}$), respectively. The movement of commodities between locations is captured by the variables $\boldsymbol{y}$, while $\boldsymbol{z}$ represents the number of transport trips required between locations.

The operator's problem includes constraints related to production continuity, facility capacity, production rates, and transportation. The detailed formulations of these constraints are provided below.

Continuity of Commodities. Constraints (1)–(7) ensure the movement of processed commodities between facilities, represented by the variable $y_{i,j,p}$. Let $\sigma^{-}_{(i,p)}$ be the set of locations from which location i receives commodity p, and $\sigma^{+}_{(i,p)}$ the set to which location i sends commodity p.

The supply constraints (1) ensure that the raw materials $q^{S}_{h,p}$ supplied by each supplier $h \in V^{S}$ are transferred to producers. The warehouse flow balance constraints (2) maintain the balance of commodities entering and leaving warehouses $j \in V^{\mathcal{W}}$. Finally, the delivery constraints (3) ensure that the final products q^{C}_{kp} are delivered to customers $k \in V^{C}$.

$$q^{S}_{hp} = \sum_{i \in \sigma^{+}_{(hp)}} y_{hip} \qquad \forall h \in V^{S}, \forall p \in P \tag{1}$$

$$q^{\mathcal{W}}_{jp} = \sum_{i \in \sigma^{-}_{(jp)}} y_{ijp} = \sum_{k \in \sigma^{+}_{(jp)}} y_{jkp} \qquad \forall j \in V^{\mathcal{W}}, \forall p \in P \tag{2}$$

$$q^{C}_{kp} = \sum_{j \in \sigma^{-}_{(kp)}} y_{jkp} \qquad \forall k \in V^{C}, \forall p \in P \tag{3}$$

$$y_{ijp} \geq 0 \qquad \forall (i,j) \in E, \forall p \in P \tag{4}$$

Constraints (5) ensure that the sum of the delivered amount q^C_{kp} and the unfulfilled amount $\bar{q}^C_{kp}$ of final products equals the customer demand D^C_{kp}.

$$q^C_{kp} + \bar{q}^C_{kp} = D^C_{kp} \qquad \forall k \in V^C, \forall p \in P \tag{5}$$

$$q^C_{kp} \geq 0 \qquad \forall k \in V^C, \forall p \in P \tag{6}$$

$$\bar{q}^C_{kp} \geq 0 \qquad \forall k \in V^C, \forall p \in P \tag{7}$$

Production Rate. Constraints (8) and (9) regulate the production rate of facilities $i \in V^{\mathcal{P}}$ for each commodity. The Bill of Materials (BoM) defines two parameters: G^{In}_{bp} and G^{Out}_{bp}, representing the quantities of commodity $p \in P$ consumed and produced per production step $b \in B$. These constraints adjust the production rate based on the required inputs, using the commodity flow variables y_{ijp}.

$$\sum_{b \in B} q^{\mathcal{P}}_{ib} \cdot G^{In}_{bp} \leq \sum_{h \in n^-(ip)} y_{hip} \qquad \forall i \in V^{\mathcal{P}}, \forall p \in P \tag{8}$$

$$\sum_{b \in B} q^{\mathcal{P}}_{ib} G^{Out}_{bp} \geq \sum_{j \in n^+(i,p)} y_{ijp} \qquad \forall i \in V^{\mathcal{P}}, \forall p \in P \tag{9}$$

Transportation. The transportation cost is determined by the average number of trips required to move commodities between location pairs. For commodity p, λ_p represents the standardized transportation capacity. Let $M_{(i,j)}$ be the set of available transportation modes between nodes i and j, with μ_m denoting the average load size per trip for mode m. Using μ_m and λ_p, Constraints (10) estimate the number of trips required for each mode m between locations $(i,j) \in E$.

$$\sum_{p \in P_{(i,j)}} y_{ijp} \cdot \lambda_p \leq \sum_{m \in M_{(i,j)}} z_{ijm} \cdot \mu_m \qquad \forall (i,j) \in E \tag{10}$$

$$z_{ijm} \geq 0 \qquad \forall (i,j) \in E, m \in M \tag{11}$$

Facility Capacity. The facility capacity constraints (12)–(15) ensure that the quantities of commodities do not exceed the capacities of suppliers, producers, or warehouses, as defined by the parameters Q^S_{hp}, $Q^{\mathcal{P}}_{ib}$, and $Q^{\mathcal{W}}_{jp}$.

$$q^S_{hp} \leq Q^S_{hp} \qquad \forall h \in V^S, \forall p \in P \tag{12}$$

$$q^{\mathcal{P}}_{ib} \leq Q^{\mathcal{P}}_{ib} \qquad \forall i \in V^{\mathcal{P}}, \forall b \in B \tag{13}$$

$$q^{\mathcal{W}}_{jp} \leq Q^{\mathcal{W}}_{jp} \qquad \forall j \in V^{\mathcal{W}}, \forall p \in P \tag{14}$$

$$q^S_{hp}, q^{\mathcal{P}}_{i,b}, q^{\mathcal{W}}_{jp} \geq 0 \qquad \forall h \in V^S, \forall i \in V^{\mathcal{P}}, \forall j \in V^{\mathcal{W}}, \forall p \in P, \forall b \in B \tag{15}$$

3.3. Disruption

The disruptor agent D makes decisions represented by the vector $\boldsymbol{x_A} = \begin{bmatrix} \boldsymbol{\phi}^S & \boldsymbol{\phi}^{\mathcal{P}} & \boldsymbol{\phi}^{\mathcal{W}} & \boldsymbol{\psi}^S & \boldsymbol{\psi}^{\mathcal{P}} \end{bmatrix}$, where $\boldsymbol{\phi}^S$, $\boldsymbol{\phi}^{\mathcal{P}}$, and $\boldsymbol{\phi}^{\mathcal{W}}$ are binary variables indicating the full disablement of a supplier (S), producer ($\mathcal{P}$), or warehouse ($\mathcal{W}$), respectively. Partial disruptions at facilities are captured by $\boldsymbol{\psi}^S$ and $\boldsymbol{\psi}^{\mathcal{P}}$, representing disruption levels for suppliers and producers.

We quantify partial disruptions using disruption impact levels $f \in F(i)$, where u_f represents the percentage of capacity lost due to failure f. These variables adjust facility capacities to account for both partial and complete disruptions. Consequently, constraints (12)–(14) are replaced by constraints (16)–(18) to reflect the impact of disruptions on supply chain operations.

$$q^S_{hp} \leq Q^S_{hp} \min(1 - \phi^S_h, 1 - u_f \psi^S_{hpf}) \qquad \forall f \in F(i), \forall h \in V^S, \forall p \in P \tag{16}$$

$$q^{\mathcal{P}}_{ib} \leq Q^{\mathcal{P}}_{ib} \min(1 - \phi^{\mathcal{P}}_i, 1 - u_f \psi^{\mathcal{P}}_{ibf}) \qquad \forall f \in F(i), \forall i \in V^{\mathcal{P}}, \forall b \in B \tag{17}$$

$$q^{\mathcal{W}}_{jp} \leq Q^{\mathcal{W}}_{jp}(1 - \phi^{\mathcal{W}}_j) \qquad \forall j \in V^{\mathcal{W}}, \forall p \in P \tag{18}$$

In constraints (16)–(18), the min function manages multiple capacity-limiting terms. The term $Q^{\cdot}_{i,p}(1-\phi^{\cdot}_i)$ reduces facility i's capacity for commodity p to zero if fully disabled. Similarly, the terms $Q^S_{ip}(1 - u_f \psi^S_{ipf})$ and $Q^{\mathcal{P}}_{ip}(1 - u_f \psi^{\mathcal{P}}_{ipf})$ represent the capacity reduction due to partial disruptions.

For each location $i \in V$, the function $\Theta(i)$ quantifies the disruption risk as a scalar. Using this, we define $\bar{C}_h$ as the cost of disabling facility h, and $\tilde{C}_{hpf}$ as the cost of disrupting the flow of commodity p due to incident f at facility h. The total disruptor budget, Γ^D, is computed based on these costs, with constraint (19) ensuring that disruptions stay within the budget β^D.

$$\begin{aligned} \Gamma^D = & \sum_{h \in V^S} \bar{C}_h \phi^S_h + \sum_{i \in V^{\mathcal{P}}} \bar{C}_i \phi^{\mathcal{P}}_i + \sum_{j \in V^{\mathcal{W}}} \bar{C}_j \phi^{\mathcal{W}}_j \\ & + \sum_{h \in V^S} \sum_{f \in F} \sum_{p \in P} \tilde{C}_{hpf} \psi^S_{hpf} + \sum_{i \in V^{\mathcal{P}}} \sum_{f \in F} \sum_{b \in B} \tilde{C}_{ibf} \psi^{\mathcal{P}}_{ibf} \leq \beta^D \end{aligned} \tag{19}$$

Constraints (20)–(22) define the domains of the variables:

$$\phi_k^{\mathcal{T}} \in \{0,1\} \quad \forall k \in V^{\mathcal{T}}, \quad V^{\mathcal{T}} = V^S \cup V^{\mathcal{P}} \cup V^{\mathcal{W}} \tag{20}$$

$$\psi_{hpf}^S \in \{0,1\} \quad \forall h \in V^S, \forall p \in P, \forall f \in F \tag{21}$$

$$\psi_{ibf}^{\mathcal{P}} \in \{0,1\} \quad \forall i \in V^{\mathcal{P}}, \forall b \in B, \forall f \in F \tag{22}$$

3.4. Resilience strategies

The decision-making process of the resilient agent $\mathcal{R}$ involves two key strategies: adding redundancy (e.g., multi-sourcing, redundant production and storage capacity) and enhancing production flexibility (e.g., flexible sourcing and production chains). In this problem, production flexibility is integrated into the production graph $\tilde{G}$. All decisions, including those related to redundancy, are captured by the vector $\boldsymbol{x}^{\boldsymbol{D}} = \begin{bmatrix}\boldsymbol{x}^S & \boldsymbol{x}^{\mathcal{P}} & \boldsymbol{x}^{\mathcal{W}}\end{bmatrix}$, where $\boldsymbol{x}^S$, $\boldsymbol{x}^{\mathcal{P}}$, and $\boldsymbol{x}^{\mathcal{W}}$ are binary variables that determine the establishment of facility locations for suppliers ($h \in V^S$), producers ($i \in V^{\mathcal{P}}$), and warehouses ($j \in V^{\mathcal{W}}$).

To incorporate these design decisions, we modify the facility capacity constraints (16)–(18). The revised constraints ensure that a facility's capacity for process p can only be utilized if the facility is included in the system design through the binary variable $x_i^{\cdot}$. The modified constraints are:

$$q_{hp}^S \le Q_{hp}^S \min(x_h^S, 1-\phi_h^S, 1-u_f\psi_{hpf}^S) \qquad \forall f \in F, h \in V^S, p \in P \tag{23}$$

$$q_{ib}^{\mathcal{P}} \le Q_{ib}^{\mathcal{P}} \min(x_i^{\mathcal{P}}, 1-\phi_i^{\mathcal{P}}, 1-u_f\psi_{ibf}^{\mathcal{P}}) \qquad \forall f \in F, i \in V^{\mathcal{P}}, b \in B \tag{24}$$

$$q_{jp}^{\mathcal{W}} \le Q_{jp}^{\mathcal{W}} \min(x_j^{\mathcal{W}}, 1-\phi_j^{\mathcal{W}}) \qquad \forall j \in V^{\mathcal{W}}, p \in P \tag{25}$$

We assume a limited budget for improving system resilience, denoted by $\beta^{\mathcal{R}}$. For each decision, the parameter C_i represents the cost of implementing improvements at location $i \in V$. Constraint (26) ensures that the total resilience improvement cost, $\Gamma^{\mathcal{R}}$, stays within the budget $\beta^{\mathcal{R}}$. Constraints (27) define the domain of the decision variables.

$$\Gamma^{\mathcal{R}} = \sum_{h \in V^S} C_h x_h^S + \sum_{i \in V^{\mathcal{P}}} C_i x_i^{\mathcal{P}} + \sum_{j \in V^{\mathcal{W}}} C_j x_j^{\mathcal{W}} \le \beta^{\mathcal{R}} \tag{26}$$

$$x_h^S \in \{0,1\}, \forall h \in V^S, x_i^{\mathcal{P}} \in \{0,1\} \forall i \in V^{\mathcal{P}}, x_j^{\mathcal{W}} \in \{0,1\} \forall j \in V^{\mathcal{W}} \tag{27}$$

3.5. Optimization model

Based on the above description, the formulation of the $\mathcal{ODR}$ problem is presented below.

$$\mathcal{ODR} \quad \min_{\boldsymbol{x}^{\mathcal{R}}} \max_{\boldsymbol{x}^{\boldsymbol{D}}} \min_{\boldsymbol{x}^{\mathcal{O}}} \quad \Gamma^{\mathcal{O}} = \rho^c \cdot \Gamma^{cost} + \rho^r \cdot \Gamma^{loss}$$

s.t.

Operator Constraints	(1) – (11), (23) – (25)
Disruptor Constraints	(19) – (22)
Resilience Designer Constraints	(26) – (27)

In $\mathcal{ODR}$, the objective function Γ^O evaluates supply chain performance by combining *operational costs* (Γ^{cost}) and *penalty costs* for unmet demand (Γ^{loss}). The parameters ρ^c and ρ^r, with $\rho^c + \rho^r = 1$, balance these costs. *Penalty costs* are incurred for undelivered quantities $\tilde{q}_{kp}^C$ and are weighted by the penalty rate $\tilde{\Pi}_{kp}$:

$$\Gamma^{loss} = \sum_{k \in V^C} \sum_{p \in P} \tilde{\Pi}_{kp} \tilde{q}_{kp}^C \tag{28}$$

Operational costs include fixed, process, and transport costs:

$$\Gamma^{cost} = \Gamma^{fixed} + \Gamma^{proc} + \Gamma^{trans} \tag{29}$$

Fixed costs cover rent and administrative expenses for suppliers, producers, and warehouses, and are calculated as:

$$\Gamma^{fixed} = \sum_{h \in V^S} \bar{\Pi}_h x_h^S + \sum_{i \in V^{\mathcal{P}}} \bar{\Pi}_i x_i^{\mathcal{P}} + \sum_{j \in V^{\mathcal{W}}} \bar{\Pi}_j x_j^{\mathcal{W}} \tag{30}$$

where x_h^S, $x_i^{\mathcal{P}}$, and $x_j^{\mathcal{W}}$ are binary variables indicating the use of each facility. Process costs are tied to the supply, production, and storage of commodities:

$$\Gamma^{proc} = \sum_{h \in V^S} \sum_{p \in P} \hat{\Pi}_{hp}^S q_{hp}^S + \sum_{i \in V^{\mathcal{P}}} \sum_{b \in B} \hat{\Pi}_{ib}^{\mathcal{P}} q_{ib}^{\mathcal{P}} + \sum_{j \in V^{\mathcal{W}}} \sum_{p \in P} \bar{\Pi}_{jp}^{\mathcal{W}} q_{jp}^{\mathcal{W}} \tag{31}$$

Transport costs are associated with moving commodities between locations:

$$\Gamma^{trans} = \sum_{(i,j)\in E} \sum_{m\in M_{(i,j)}} \check{\Pi}_{ijm} z_{ijm} \tag{32}$$

where z_{ijm} is the number of trips between locations i and j using transport mode m, and $\check{\Pi}_{ijm}$ represents the associated transport cost.

4. Resolution approach

We propose a decomposition approach to solve the tri-level optimization problem ($\mathcal{ODR}$), inspired by the methods of Alderson et al. (2011) and Ghorbani-Renani et al. (2021). Our approach decomposes the tri-level $\mathcal{ODR}$ model into two interconnected problems: a single-level master problem ($\mathcal{ODR}$-Master), which provides a lower bound, and a bi-level disruptor sub-problem ($\mathcal{ODR}$-Sub), which defines the upper bound. This decomposition facilitates a more tractable solution to the hierarchical decision model in $\mathcal{ODR}$. Although the iterative structure of our decomposition resembles classical Benders or L-shaped methods, the approaches differ fundamentally in formulation and applicability. Benders decomposition is suited for two-stage problems with a linear recourse subproblem, leveraging dual solutions to generate optimality cuts. In contrast, our model adopts a tri-level structure, where the lower two levels form a bilevel adversarial game between the disruptor and the operator. To solve this, we reformulate the bilevel subproblem as a single-level mixed-integer quadratic program (MIQP) via dualization. This enables tractable identification of worst-case disruption scenarios—an element not addressed by classical Benders or L-shaped frameworks.

For a given disruption vector $\hat{\boldsymbol{x}}^{\boldsymbol{D}}_{\boldsymbol{k}}$, there exists a corresponding operational response $\hat{\boldsymbol{x}}^{\mathcal{O}}_{\boldsymbol{k}}$, forming the pair $(\hat{\boldsymbol{x}}^{\boldsymbol{D}}_{\boldsymbol{k}}, \hat{\boldsymbol{x}}^{\mathcal{O}}_{\boldsymbol{k}})$. The $\mathcal{ODR}$-Master problem determines the optimal system design $\overset{*}{\boldsymbol{x}}^{\boldsymbol{\mathcal{R}}}$ for a given set of potential disruptions, yielding the disruption-response pair $(\overset{*}{\boldsymbol{x}}^{\boldsymbol{D}}, \overset{*}{\boldsymbol{x}}^{\mathcal{O}})$. Conversely, the $\mathcal{ODR}$-Sub problem identifies the worst-case disruption vector $\overset{*}{\boldsymbol{x}}^{\boldsymbol{D}}$ for a fixed system design $\hat{\boldsymbol{x}}^{\boldsymbol{\mathcal{R}}}$. This iterative exchange between the master and sub-problem allows for continuous refinement of the solution.

In Algorithm 1, the iterative process begins by initializing an empty set of disruption vectors, starting with an initial feasible disruption vector $\hat{\boldsymbol{x}}^{\boldsymbol{D}}_{\boldsymbol{0}}$ (e.g., "no disruption"). The algorithm first solves the $\mathcal{ODR}$-Master problem for the initial disruption vector to obtain the system design $\boldsymbol{x}^{\boldsymbol{\mathcal{R}}}_{1}$ and an initial operational cost z. The initial lower bound is set to $z^{LO} = z$, and the upper bound is initialized to infinity, $z^{UP} = +\infty$.

At each iteration, the algorithm first solves the $\mathcal{ODR}$-Sub problem for the current system design $\hat{\boldsymbol{x}}^{\boldsymbol{\mathcal{R}}}_{\boldsymbol{K}}$ to identify the worst-case disruption vector $\boldsymbol{x}^{\boldsymbol{D}}_{\boldsymbol{K}}$, which maximizes the operational cost. If this cost is lower than the current upper bound, the upper bound is updated, $z^{UP} \leftarrow z$, and the optimal design and disruption vectors are updated to $\overset{*}{\boldsymbol{x}}^{\boldsymbol{\mathcal{R}}}$ and $\overset{*}{\boldsymbol{x}}^{\boldsymbol{D}}$, respectively.

The set of disruption vectors is then updated by adding the newly found disruption vector to the set: $\hat{\boldsymbol{x}}^{\boldsymbol{D}}_{\boldsymbol{k}} \leftarrow \hat{\boldsymbol{x}}^{\boldsymbol{D}}_{\boldsymbol{k}} \cup \{\boldsymbol{x}^{\boldsymbol{D}}_{\boldsymbol{K}}\}$. The $\mathcal{ODR}$-Master problem is re-solved for the updated set of disruption vectors to find the new optimal system design $\boldsymbol{x}^{\boldsymbol{\mathcal{R}}}_{\boldsymbol{K+1}}$, and the lower bound is updated if necessary, $z^{LO} \leftarrow z$.

This process repeats until the gap between the upper and lower bounds, $z^{UP} - z^{LO}$, falls below a predefined tolerance ϵ, or until the iteration limit K_{MAX} is reached. This guarantees convergence to an ϵ-optimal solution with a bounded suboptimality gap. Upon termination, the algorithm solves the operator problem (**mO**) to obtain the optimal operational response $\overset{*}{\boldsymbol{x}}^{\mathcal{O}}$, given the optimal design $\overset{*}{\boldsymbol{x}}^{\boldsymbol{\mathcal{R}}}$ and the worst-case disruption vector $\overset{*}{\boldsymbol{x}}^{\boldsymbol{D}}$. The final output is the triplet $(\overset{*}{\boldsymbol{x}}^{\boldsymbol{\mathcal{R}}}, \overset{*}{\boldsymbol{x}}^{\boldsymbol{D}}, \overset{*}{\boldsymbol{x}}^{\mathcal{O}})$.

Algorithm 1: $\mathcal{ODR}$ Iterative Resolution

Input: ϵ, K_{MAX}
Output: $(\overset{*}{\boldsymbol{x}}^{\boldsymbol{\mathcal{R}}}, \overset{*}{\boldsymbol{x}}^{\boldsymbol{D}}, \overset{*}{\boldsymbol{x}}^{\mathcal{O}})$
Initialize $\hat{\boldsymbol{x}}^{\boldsymbol{D}}_{\boldsymbol{0}} \leftarrow \{\emptyset\}$, select $\hat{\boldsymbol{x}}^{\boldsymbol{D}}_{\boldsymbol{0}}$, solve $\mathcal{ODR} - Master$ to get $\boldsymbol{x}^{\boldsymbol{\mathcal{R}}}_{1}$ and z^*, set $z^{LO} \leftarrow z^*$, $z^{UP} \leftarrow +\infty$, $K \leftarrow 1$.
while $z^{UP} - z^{LO} > |z^{LO}| \cdot \epsilon$ ***and*** $K < K_{MAX}$ **do**
  Solve $\mathcal{ODR} - Sub$ for $\hat{\boldsymbol{x}}^{\boldsymbol{\mathcal{R}}}_{\boldsymbol{K}}$ to get $\boldsymbol{x}^{\boldsymbol{D}}_{\boldsymbol{K}}$ and z;
  if $z < z^{UP}$ **then**
    $z^{UP} \leftarrow z$, $\overset{*}{\boldsymbol{x}}^{\boldsymbol{\mathcal{R}}} \leftarrow \hat{\boldsymbol{x}}^{\boldsymbol{\mathcal{R}}}_{\boldsymbol{K}}$, $\overset{*}{\boldsymbol{x}}^{\boldsymbol{D}} \leftarrow \boldsymbol{x}^{\boldsymbol{D}}_{\boldsymbol{K}}$;
  end
  Update set: $\hat{\boldsymbol{x}}^{\boldsymbol{D}}_{\boldsymbol{K}} \leftarrow \hat{\boldsymbol{x}}^{\boldsymbol{D}}_{\boldsymbol{K}} \cup \{\boldsymbol{x}^{\boldsymbol{D}}_{\boldsymbol{K}}\}$;
  Solve $\mathcal{ODR} - Master$ for $\hat{\boldsymbol{x}}^{\boldsymbol{D}}_{\boldsymbol{K}}$ to get $\boldsymbol{x}^{\boldsymbol{\mathcal{R}}}_{\boldsymbol{K+1}}$ and z;
  if $z > z^{LO}$ **then**
    $z^{LO} \leftarrow z$;
  end
  Increment K.
end
Solve **mO** for $\overset{*}{\boldsymbol{x}}^{\mathcal{O}}$ given $(\overset{*}{\boldsymbol{x}}^{\boldsymbol{\mathcal{R}}}, \overset{*}{\boldsymbol{x}}^{\boldsymbol{D}})$;
return $(\overset{*}{\boldsymbol{x}}^{\boldsymbol{\mathcal{R}}}, \overset{*}{\boldsymbol{x}}^{\boldsymbol{D}}, \overset{*}{\boldsymbol{x}}^{\mathcal{O}})$.

4.1. Master problem $\mathcal{ODR}$-master

The $\mathcal{ODR}$-Master problem optimizes the system design, $\overset{*}{\boldsymbol{x}}^{\boldsymbol{\mathcal{R}}}$, for a given set of disruption vectors, $\hat{\boldsymbol{x}}_{\boldsymbol{k}}^{\boldsymbol{\mathcal{D}}}$. In addition to the design variables, it introduces a continuous variable, Z, which represents an upper bound on the worst-case system performance across all disruption scenarios. The problem also includes operational variables, $\boldsymbol{x}_{\boldsymbol{k}}^{\mathcal{O}}$, which describe the system's response to each disruption vector $\hat{\boldsymbol{x}}_{\boldsymbol{k}}^{\boldsymbol{\mathcal{D}}}$.

The objective of the master problem is to minimize Z, subject to several constraints. The design variables, $\boldsymbol{x}^{\boldsymbol{\mathcal{R}}}$, are restricted to the feasible design space $X^{\mathcal{R}}$, ensuring that the selected design satisfies all system requirements. The operational variables, $\boldsymbol{x}_{\boldsymbol{k}}^{\mathcal{O}}$, must satisfy the operational constraints defined by $X^{\mathcal{O}}(\boldsymbol{x}^{\boldsymbol{\mathcal{R}}}, \hat{\boldsymbol{x}}_{\boldsymbol{k}}^{\boldsymbol{\mathcal{D}}})$ for each disruption scenario k. Finally, Z must be greater than or equal to the total system cost, $\Gamma^{\text{total}}(\boldsymbol{x}^{\boldsymbol{\mathcal{R}}}, \hat{\boldsymbol{x}}_{\boldsymbol{k}}^{\boldsymbol{\mathcal{D}}}, \boldsymbol{x}_{\boldsymbol{k}}^{\mathcal{O}})$, for every disruption-response pair $(\hat{\boldsymbol{x}}_{\boldsymbol{k}}^{\boldsymbol{\mathcal{D}}}, \boldsymbol{x}_{\boldsymbol{k}}^{\mathcal{O}})$.

Thus, the master problem is formulated as follows:

$$[\mathcal{ODR} - Master]$$

$$\min_{Z, \boldsymbol{x}^{\boldsymbol{\mathcal{R}}}, \boldsymbol{x}_1^{\mathcal{O}}, \ldots, \boldsymbol{x}_K^{\mathcal{O}}} \quad Z \tag{33}$$

$$\text{s.t.} \quad \boldsymbol{x}^{\boldsymbol{\mathcal{R}}} \in X^{\mathcal{R}} \tag{34}$$

$$\boldsymbol{x}_{\boldsymbol{k}}^{\mathcal{O}} \in X^{\mathcal{O}}(\boldsymbol{x}^{\boldsymbol{\mathcal{R}}}, \hat{\boldsymbol{x}}_{\boldsymbol{k}}^{\boldsymbol{\mathcal{D}}}) \quad \forall k \in K \tag{35}$$

$$Z \geq \Gamma^{\text{total}}(\boldsymbol{x}^{\boldsymbol{\mathcal{R}}}, \hat{\boldsymbol{x}}_{\boldsymbol{k}}^{\boldsymbol{\mathcal{D}}}, \boldsymbol{x}_{\boldsymbol{k}}^{\mathcal{O}}) \quad \forall k \in K \tag{36}$$

4.2. Disruptor sub-problem $\mathcal{ODR}$-sub

The $\mathcal{ODR}$-Sub problem is formulated to identify the worst-case disruption vector $\overset{*}{\boldsymbol{x}}^{\mathcal{D}}$, which maximizes the operational cost for a fixed system design $\hat{\boldsymbol{x}}^{\boldsymbol{\mathcal{R}}}$. To solve this bi-level optimization problem, we employ a "dualize-and-combine" approach based on the duality theory of Dempe and Zemkoho (2020). This method reformulates the bi-level structure of $\mathcal{ODR}$-Sub into a single-level mixed-integer quadratic problem (MIQP) by replacing the inner minimization problem (the operator's model) with its dual maximization.

Since the operator's model is linear, this reformulation transforms the sub-problem into a tractable MIQP. The objective of $\mathcal{ODR}$-Sub is to find the disruption vector that causes the most damage to the operator's performance while respecting the constraints of the fixed system design.

5. Computational analysis

We conduct our experiments using Python and Gurobi 11.0.2. All experiments are carried out on a computer with a Core i5 processor and 16 GB of RAM. In Section 5.1, we report the computational performance of our decomposition approach. In Section 5.2, we investigate the impact of having a flexible production chain on improving supply chain resilience. Finally, in Section 5.3, we present a resilience analysis of a pharmaceutical supply chain considering climate-related hazards.

5.1. Computational performance

We evaluate the computational performance of our proposed decomposition approach using 12 instances, generated by combining four distinct production chain layouts with three network sizes. The production chains range from a simple single-step process (`Simple`) to a complex multi-input, multi-output network (`Complex`), varying in the number of production steps and commodities. To capture different levels of complexity and scale, these production chains are paired with three network sizes—`Small`, `Medium`, and `Large`—representing local to global supply chains. Table 2 summarizes the characteristics of each instance, detailing the physical network and production processes, including the number of suppliers ($|S|$), producers ($|P|$), warehouses ($|\mathcal{W}|$), customers ($|C|$), production steps ($|B|$), and commodities ($|P|$) in each configuration.

For each configuration, we assess computational performance by varying both disruption and resilience budgets. These budgets are expressed in relative terms, with disruption budgets representing the resources available to disrupt operations and resilience budgets reflecting the resources allocated for fortification. In the experiment, the cost hierarchy for establishing new facilities is structured as follows: adding a new supplier incurs the lowest cost, followed by establishing a new warehouse, while adding a new producer requires the highest cost.

Table 3 details the disruption impact levels and the corresponding number of new facilities that can be established under each resilience budget. Disruptions are categorized by severity, ranging from `Mild` (10% reduction in capacity) to `Catastrophe` (complete shutdown), and are quantified by the disruptor budget ($\Gamma^{\mathcal{D}}$). Similarly, the resilience budget ($\Gamma^{\mathcal{R}}$) determines the number of new facilities that can be introduced to enhance the supply chain's resilience.

Table 4 summarizes the computational performance of the model, reporting both the solution time (in seconds) and the optimality gap (in %) for the generated instances. The rows correspond to the different production chain configurations, organized by disruption budget, while the columns represent network sizes, organized by resilience design budget.

Table 2
Computational performance instances.

Network-Production	$\|S\|$	$\|\mathcal{P}\|$	$\|\mathcal{W}\|$	$\|C\|$	$\|B\|$	$\|P\|$
`Small-Simple`	10	5	5	10	1	3
`Small-LinSingl`	10	5	5	10	5	8
`Small-LinMulti`	10	5	5	10	15	24
`Small-Complex`	10	5	5	10	43	74
`Medium-Simple`	30	15	15	50	1	3
`Medium-LinSingl`	30	15	15	50	5	8
`Medium-LinMulti`	30	15	15	50	15	24
`Medium-Complex`	30	15	15	50	43	74
`Large-Simple`	50	25	25	200	1	3
`Large-LinSingl`	50	25	25	200	5	8
`Large-LinMulti`	50	25	25	200	15	24
`Large-Complex`	50	25	25	200	43	74

Table 3
Scenarios - Disruptor and Design Budgets and their relative resource value.

	Disruption Level					New Facilities		
$\Gamma^{\mathcal{D}}$	Minor	Heavy	Major	Fatal	$\Gamma^{\mathcal{R}}$	$\|S\|$	$\|\mathcal{P}\|$	$\|\mathcal{W}\|$
None	0	0	0	0	None	0	0	0
Mild	1	0	0	0	Min.	1	0	0
Mod.	25	5	1	0	Mod.	10	0	1
Sev.	50	12	2	0	Ext.	100	1	10
Cat.	200	50	8	2	Glob.	500	5	50

The results show that the model is capable of solving a wide range of realistically sized instances within a reasonable time frame. For all cases, the minimum optimality gap (ε) was set at 10^{-5}, with a maximum computation time of 90 min (5400 s). Out of the 300 instances tested, 291 were successfully solved within this time limit.

Three key factors were identified as influencing computational performance: (1) network size, (2) disruption budget, and (3) resilience design budget. Larger networks increase the number of design decisions ($\mathbf{x}^{\boldsymbol{R}}$), which directly impacts the size of the $\mathcal{ODR}$-Master problem and computational performance. However, the complexity of the production chain (in terms of the number of steps and commodities) had little effect on solution times. While more complex chains require additional operational decisions ($\mathbf{x}^{\boldsymbol{D}}$), this did not significantly prolong computation.

Additionally, higher disruption and resilience design budgets (β^{D} and $\beta^{\mathcal{R}}$) generally increased computational time. Larger budgets allow for a wider range of design and disruption decisions, thus expanding the solution space and increasing the time required to find the optimal solution. Conversely, smaller budgets impose stricter constraints, enabling the model to eliminate infeasible solutions more quickly, thereby reducing computation times.

5.2. Production chain flexibility and its impact on resilience

In this subsection, we evaluate the resilience of a steel manufacturing supply chain, focusing on the impact of both production chain and physical network flexibility. We define four instances that vary based on these flexibilities. The base case, I_0, models a single-path production chain with no physical flexibility, where `crude coal` and `crude iron` are transformed into `finished goods` through a linear process (see Fig. 2). The network consists of 2 suppliers, 4 producers, 10 warehouses, and 100 customers with randomized locations.

In I_1, physical network flexibility is introduced by adding potential facilities, expanding the network to 10 suppliers, 16 producers, and 30 warehouses, while maintaining the same customer base. In I_2, production chain flexibility is incorporated by introducing alternative paths (represented by dashed lines in Fig. 2), such as using `iron pellets`, `direct reduced iron` (DRI), and an `electric arc furnace`, which substitutes `scrap metal` for coal. The physical network remains the same as in I_0. Finally, I_3 combines both the production chain flexibility from I_2 and the physical network flexibility from I_1, representing the most comprehensive flexibility scenario. To assess the effectiveness of the proposed designs under different disruptions, we introduce two key metrics: system performance and system resilience. System performance (P) measures how well a design $\boldsymbol{x}^{\boldsymbol{R}}$ fulfills the demand under a disruption scenario $\boldsymbol{x}^{\boldsymbol{D}}$, expressed as the total percentage of fulfilled demand for each end-user $k \in L^C$:

$$\mathrm{P}(\boldsymbol{x}^{\boldsymbol{D}}, \boldsymbol{x}^{\boldsymbol{R}}) = \sum_{k \in L^C} \sum_{p \in P} \frac{q^C_{kp}}{D^C_{kp}}$$

Table 4
Computational results.

Prod.	Net. Size $\Gamma^R/\ \Gamma^D$	Small					Medium					Large					
			None	Min.	Mod.	Ext.	Glb	None	Min.	Mod.	Ext.	Glb	None	Min.	Mod.	Ext.	Glb
Simple	None	Time (s)	0	0.01	0.01	0.02	0.01	0.01	0.01	0.10	0.42	0.12	0.04	0.06	0.39	2.06	2.62
		Gap (%)	0	0	0	0	0	0	0	0	0	0	0	0	0	0	0
	Mild	Time (s)	0.03	0.18	0.24	0.10	0.08	0.13	1.12	3.78	5.59	0.60	0.53	2.20	71.39	3.88	4.43
		Gap (%)	0	0	0	0	0	0	0	0	0	0	0	0	0	0	0
	Mod.	Time (s)	0.03	0.15	0.30	0.12	0.12	0.12	0.59	41.98	261.42	0.81	0.47	2.25	392.79	3.90	4.44
		Gap (%)	0	0	0	0	0	0	0	0	0	0	0	0	0	0	0
	Sev.	Time (s)	0.04	0.14	0.26	0.19	0.12	0.12	0.63	42.23	263.82	0.73	0.46	2.25	382.06	4.05	4.70
		Gap (%)	0	0	0	0	0	0	0	0	0	0	0	0	0	0	0
	Cat.	Time (s)	0.03	0.24	0.24	2.49	5.34	0.13	1.63	1.49	**5400**	1787.82	0.53	5.34	5.88	**5400**	5400
		Gap (%)	0	0	0	0	0	0	0	0	**173.64**	0	0	0	0	**174.23**	0.58
LinSingl	None	Time (s)	0.01	0.01	0.02	0.02	0.02	0.01	0.02	0.22	0.32	0.14	0.06	0.07	0.29	1.43	1.77
		Gap (%)	0	0	0	0	0	0	0	0	0	0	0	0	0	0	0
	Mild	Time (s)	0.06	0.53	0.77	0.57	0.69	0.21	1.11	4.41	12.80	9.48	0.73	2.96	1023.97	586.64	387.14
		Gap (%)	0	0	0	0	0	0	0	0	0	0	0	0	0	0	0
	Mod.	Time (s)	0.06	0.41	0.62	2.60	0.59	0.29	1.15	5.86	84.93	21.81	0.61	3.00	57.81	**5400**	5190.04
		Gap (%)	0	0	0	0	0	0	0	0	0	0	0	0	0	**50.96**	0.21
	Sev.	Time (s)	0.05	0.24	0.55	1.38	0.81	0.20	0.88	5.66	11.84	11.38	1.62	4.60	107.02	2132.22	5283.48
		Gap (%)	0	0	0	0	0	0	0	0	0	0	0	0	0	0	0.05
	Cat.	Time (s)	0.08	0.28	0.73	3.70	4.35	0.27	1.26	6.04	2299.32	**5400**	0.68	3.10	7.71	**5400**	**5400**
		Gap (%)	0	0	0	0	0	0	0	0	0	**102.87**	0	0	0	**101.71**	**103.23**
LinMulti	None	Time (s)	0.01	0.01	0.01	0.01	0.01	0.02	0.05	0.11	0.17	1.22	0.09	0.12	0.63	2.44	2.73
		Gap (%)	0	0	0	0	0	0	0	0	0	0	0	0	0	0	0
	Mild	Time (s)	0.10	0.47	0.49	0.42	0.50	0.32	1.42	6.73	62.16	2885.99	2.37	10.10	594.24	**5400**	**5400**
		Gap (%)	0	0	0	0	0	0	0	0	0	0	0	0	0	**10.73**	**10.98**
	Mod.	Time (s)	0.22	0.49	0.47	0.75	0.49	0.42	1.59	65.08	3977.50	5357.82	2.24	16.78	4290.81	**5400**	**5400**
		Gap (%)	0	0	0	0	0	0	0	0	0	0	0	0	0	**15.08**	**66.13**
	Sev.	Time (s)	0.22	0.58	0.61	0.80	0.54	0.39	2.65	11.62	568.13	1077.06	1.24	15.65	92.26	**5400**	**5400**
		Gap (%)	0	0	0	0	0	0	0	0	0	0	0	0	0	**35.42**	**108.72**
	Cat.	Time (s)	0.31	0.93	1.47	2.39	1.42	0.54	5.25	5.13	195.72	**5400**	1.36	14.35	161.47	2857.83	**5400**
		Gap (%)	0	0	0	0	0	0	0	0	0	**35.29**	0	0	0	0	**221.10**
Complex	None	Time (s)	0.02	0.01	0.03	0.02	0.03	0.09	0.26	0.10	0.08	0.15	0.17	0.17	0.34	0.34	0.48
		Gap (%)	0	0	0	0	0	0	0	0	0	0	0	0	0	0	0
	Mild	Time (s)	0.55	2.27	2.04	2.48	2.70	1.24	4.10	4.30	3.62	3.58	2.06	9.39	24.80	77.03	1672.71
		Gap (%)	0	0	0	0	0	0	0	0	0	0	0	0	0	0	0
	Mod.	Time (s)	0.67	2.28	2.36	2.44	2.32	0.99	4.39	7.66	4.41	4.32	3.35	10.88	24.99	200.51	4175.57
		Gap (%)	0	0	0	0	0	0	0	0	0	0	0	0	0	0	0
	Sev.	Time (s)	0.44	2.16	2.19	1.96	2.05	0.88	6.42	6.60	3.62	3.59	2.50	11.37	40.83	166.07	5400
		Gap (%)	0	0	0	0	0	0	0	0	0	0	0	0	0	0	0
	Cat.	Time (s)	0.55	3.82	3.16	3.19	3.22	0.80	3.51	3.63	3.60	3.54	2.15	9.74	17.85	33.09	92.05
		Gap (%)	0	0	0	0	0	0	0	0	0	0	0	0	0	0	0

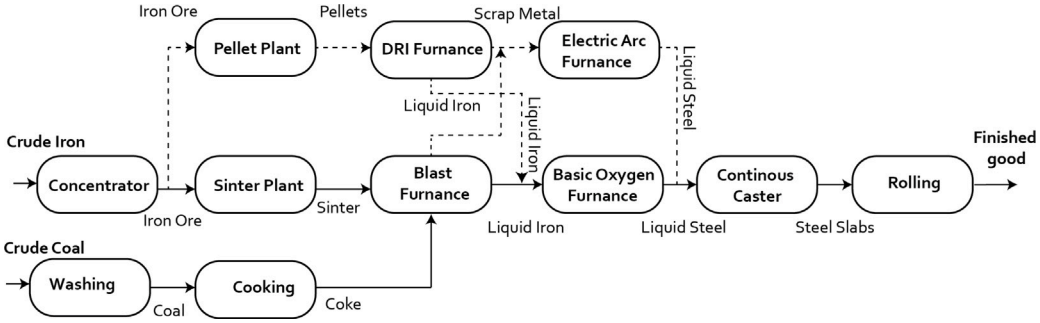

Fig. 2. Production graph for instances I_0 to I_3. Solid lines represent the single-path production chain of I_0 and I_1, while dashed lines show the additional components in I_2 and I_3. Only `Convert` nodes are shown.

System resilience (`R-score`) captures the robustness of a design by calculating the area under the performance curve (P) across varying disruption budgets. For a set of disruptor budgets α, the resilience score is computed using the trapezoidal rule:

$$\mathtt{R-score}(\boldsymbol{x}^{\boldsymbol{R}}) = \int_0^{\infty} \mathrm{P}\, d(\beta^{\mathcal{D}}) = \frac{1}{2}\sum_{\alpha}(\beta^{\mathcal{D}}_{\alpha+1} - \beta^{\mathcal{D}}_{\alpha})(\mathrm{P}_{\alpha} + \mathrm{P}_{\alpha+1})$$

System performance (P) was evaluated as a function of the disruption budget ($\beta^{\mathcal{D}}$) for both simple and complex production chains without network flexibility (instances I_0 and I_2), as shown in Fig. 3. The black line in the figure illustrates the degradation

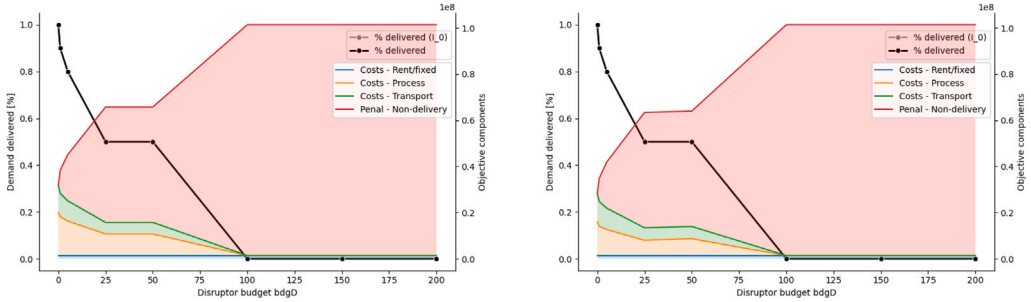

(a) Instance I_0, $\beta^{\mathcal{R}} = 0$ (b) Instance I_2, $\beta^{\mathcal{R}} = 0$

Fig. 3. Performance P and objective function components for instances I_0 and I_2.

in performance as the disruption budget increases. The left y-axis displays performance, while the right y-axis breaks down the objective function into its cost components. Similarly, Fig. 4 demonstrates the impact of network flexibility by varying the design budget ($\beta^{\mathcal{R}}$) for instances I_1 and I_3.

To assess resilience, the area under the performance curve (`R-score`) was calculated for each instance and is presented in Fig. 5. Increasing the design resource budget enhances resilience significantly, particularly when both production chain and network flexibility are incorporated. Without production chain flexibility, resilience improves by 254% at the highest design budget ($\beta^{\mathcal{R}} = 5,000,000$). When production chain flexibility is added, resilience increases by 30.6% at a smaller design budget ($\beta^{\mathcal{R}} = 1,000,000$) and by 284% at the larger budget. These findings underscore the value of combining both types of flexibility to achieve greater resilience.

5.3. Assessing resilience in a global pharmaceutical supply chain

This section outlines the expansion plan of a pharmaceutical company producing three drugs: `ProductA`, `ProductB`, and `ProductC`. These drugs are primarily sold in the US and Europe, with additional demand in Latin America, South Africa, and the Asia-Pacific region. The production process includes drug substance manufacturing, vial filling, and packaging, with raw materials sourced from biological suppliers.

`ProductA` is filled into vials of 10, 20, or 30 mg, while `ProductB` is filled into vials of 5, 10, 15, 20, or 25 mg. These vials are packed into units of 1, 2, 5, 6, or 10 and distributed globally. Fig. 6 presents a simplified version of the company's production process.

The company's supply chain consists of suppliers, production sites, warehouses, and demand cities. It operates four production facilities: `MU - UnitedStates`, `MU-Belgium`, `MU-Italy`, and `MU-Ireland`, each specializing in different production steps and products. For instance, `MU-Belgium` operates multiple filling lines, and vial packs of 5 and 10 are produced exclusively in the US, while packs of 1 and 6 are produced in Europe. Packs of 2 vials are produced in both regions.

The distribution network connects approximately 30 warehouses to 189 demand cities globally. Transportation modes include truck, rail, and sea between suppliers, producers, and warehouses, with customer deliveries primarily using Less Than Truckload (LTL) services.

To meet growing demand, particularly from Asia, the company plans to expand by adding new production sites in Germany, India, Indonesia, Egypt, and Brazil. These locations, each with different production capacities, are part of the Supply Chain Decision Network. Additionally, ten new raw material suppliers and 30 potential warehouse locations have been identified, each with distinct investment costs.

Quantifying Climate-Related Disruption. We model disruptions based on climate hazards and geopolitical risks. To assess resilience against climate risks, we assign each location i a risk score $\Theta(i)$ for each hazard r, ranging from 0 (low risk) to 1 (high risk). These scores represent the likelihood of a location being affected by a hazard before 2050. The disruption cost Γ^D for disrupting a facility i at disruption level f is given by:

$$\Gamma^D_{if} = \bar{C}_f \cdot \left(1 - \sum_{r \in R} K_{rf} \cdot \Theta(i)\right)$$

Here, $\Theta(i)$ represents the susceptibility of facility i to hazard r, and K_{rf} links each hazard to a disruption level. For example, earthquakes are more likely to cause a `FATAL` disruption, while heat may lead to `MINOR` or `HEAVY` disruptions. The level bias $\bar{C}_f$ reflects the likelihood of different disruption levels, with minor disruptions being more probable than fatal ones. Disruption levels are defined in Table 5 and range from minimal impact (−10% capacity) to total disruption.

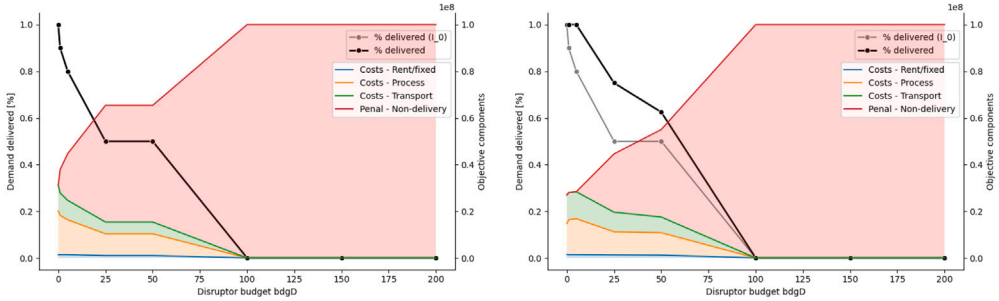

(a) Instance I_1, $\beta^{\mathcal{R}} = 1,000,000$ (b) Instance I_3, $\beta^{\mathcal{R}} = 1,000,000$

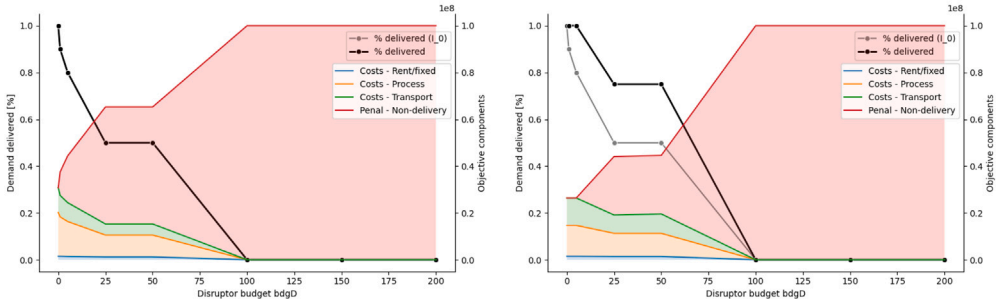

(c) Instance I_1, $\beta^{\mathcal{R}} = 2,000,000$ (d) Instance I_3, $\beta^{\mathcal{R}} = 2,000,000$

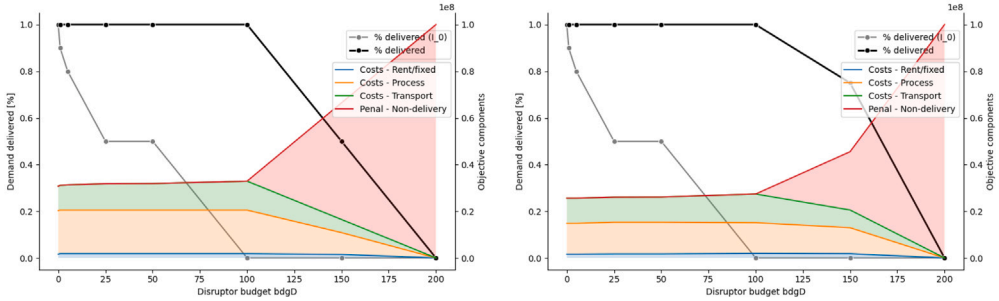

(e) Instance I_1, $\beta^{\mathcal{R}} = 5,000,000$ (f) Instance I_3, $\beta^{\mathcal{R}} = 5,000,000$

Fig. 4. Effect of physical flexibility on performance P and objective function components for instances I_1 and I_3, with various design budgets $\beta^{\mathcal{R}}$.

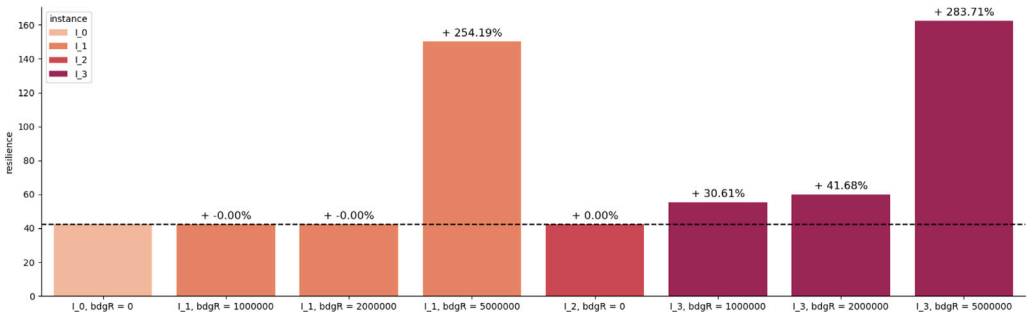

Fig. 5. Resilience score `R-score` of the difference instances and design budgets $\beta^{\mathcal{R}}$.

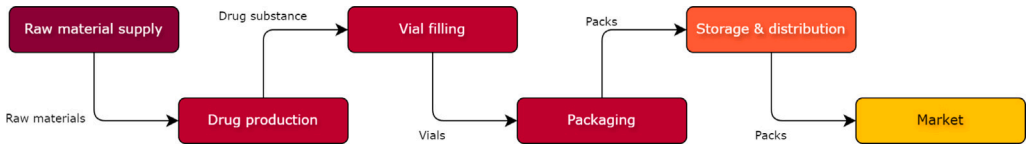

Fig. 6. Diagram of production steps.

Table 5
Climate hazard and disruption level definitions.

f	u_f	$\bar{C}_f$	Heat	Cold	Rain	Snow	Trop. Storm	Wild fire	Air Qual.	Flood	Drght	Earthq.	Hum. Confl.
MINOR	10	1	0.020	0.020	0.020	0.020	0.005	0.005	0.010	0.005	0.020	0.005	0.005
HEAVY	20	4	0.020	0.020	0.020	0.020	0.010	0.010	0.005	0.010	0.020	0.010	0.010
MAJOR	50	25	0.010	0.010	0.010	0.010	0.050	0.050	0.005	0.050	0.010	0.050	0.050
FATAL	100	100	0.005	0.005	0.005	0.005	0.050	0.050	0.001	0.050	0.010	0.050	0.050

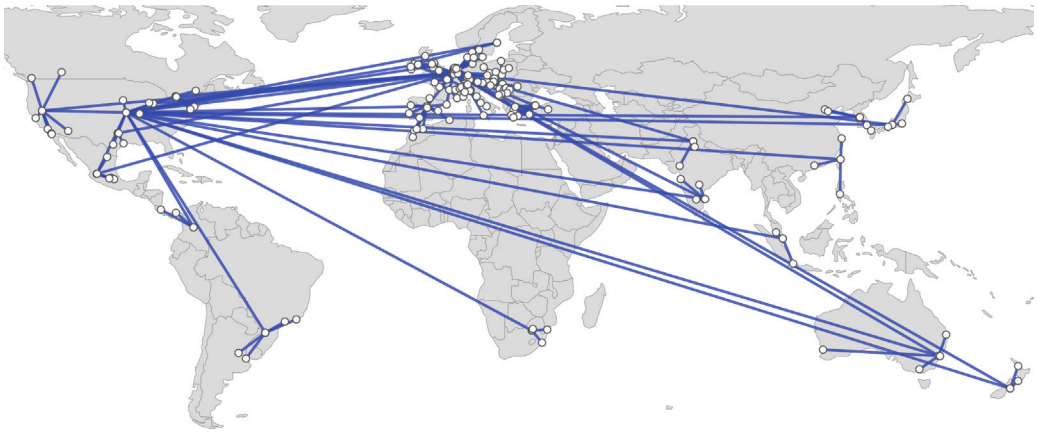

Fig. 7. Map, $\beta^D = 0$, $\beta^R = 0$.

Assessing Resilience of the Current Network. This section examines the resilience of the supply chain network by first establishing a baseline under normal operating conditions. By setting both the disruption budget (β^D) and the resilience budget (β^R) to zero, the model identifies the optimal configuration of the supply chain, as shown in Fig. 7.

Next, to understand how disruptions affect the network, we simulate various disruption scenarios by gradually increasing the disruption budget (β^D), ranging from minor ($\beta^D = 1$) to major ($\beta^D = 100$). The analysis reveals that minor disruptions have limited effects, while larger disruptions expose significant vulnerabilities, sometimes leading to a near-total breakdown of the system. Table 6 details the facilities affected at different disruption levels, highlighting how the critical nodes in the supply chain shift as the severity of disruptions increases.

For example, facilities such as `MU-Belgium PACKAGING` experience a gradual escalation from `MINOR` disruption at $\beta^D = 1$ to `FATAL` at $\beta^D = 300$, indicating its heightened vulnerability. Similarly, `MU-UnitedStates DRUGPROD` and `MU-UnitedStates PACKAGING` are heavily impacted at higher disruption budgets, marking them as critical points in the network.

Geographical vulnerabilities are spread throughout the network. US and Belgium facilities face disruptions at multiple levels, while `MU-Ireland DRUGPROD` and `MU-Italy PACKAGING` only become vulnerable at higher disruption budgets. This suggests that resilience efforts should focus on facilities with greater risk exposure, prioritizing protection for those vulnerable to a wider range of disruptions. By targeting critical nodes based on their specific risk levels, resilience strategies can be more efficiently applied.

To assess the impact of climate-adjusted disruption costs on strategic design decisions, we examine the frequency with which each facility is targeted for disruption and selected in the final network configuration across multiple scenarios. Figs. 8 and 9 report these outcomes.

The disruption frequency results indicate that critical vulnerabilities are concentrated in a small subset of facilities — particularly `MU Belgium PACKAGING` and `MU UnitedStates PACKAGING` — which are selected disproportionately across scenarios. This reflects their structural centrality and lack of operational redundancy.

Table 6
Disrupted facilities by β^D with $\beta^R = 0$.

Facility	β^D 0	1	5	25	50	100	200	300
MU Belgium PACKAGING		MINOR	MINOR	HEAVY	MAJOR			FATAL
MU UnitedStates DRUGPROD			MINOR	MINOR	HEAVY	FATAL	FATAL	
MU UnitedStates PACKAGING			HEAVY	MAJOR	MAJOR			FATAL
SU CellBoost US				MINOR	MINOR			
MU Ireland DRUGPROD				MINOR	HEAVY	MAJOR	FATAL	
WH Germany GRIESHEIM					MINOR	MINOR		
WH NETHERLANDS Nijmegen						MINOR		
MU Italy PACKAGING								FATAL

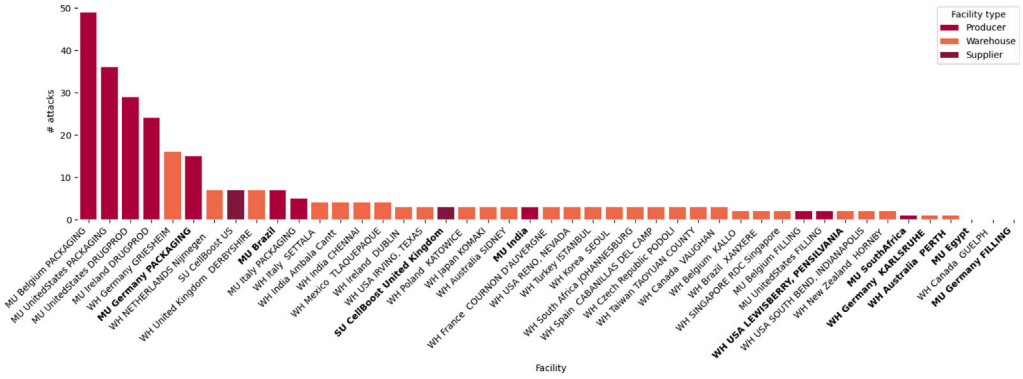

Fig. 8. Disruption frequency by facility across scenarios. Facilities in **bold** were not part of the initial network and require investment to be activated.

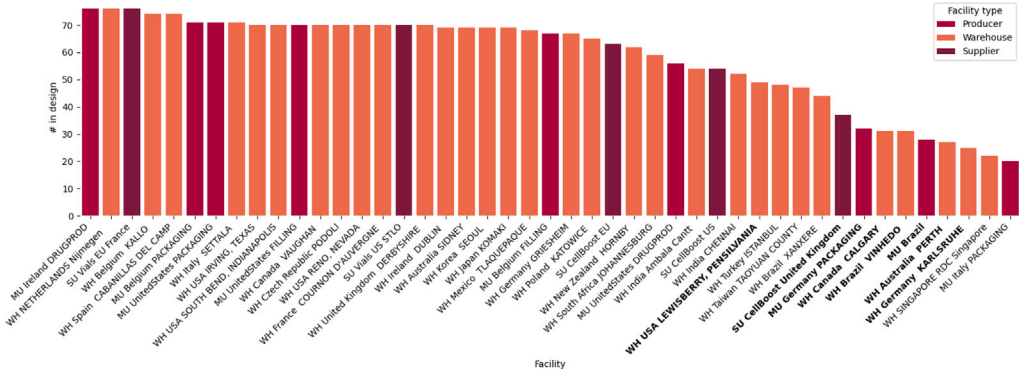

Fig. 9. Frequency of facility selection in network design across scenarios. Facilities in **bold** were not in the original network configuration.

In contrast, facility inclusion results exhibit greater dispersion, with frequent selection of both incumbent and new warehouse nodes. This suggests that, under sufficient resilience budgets, the model favors network diversification, primarily through expanded storage and distribution capacity.

Strategic Supply Chain Expansion. This section examines the firm's expansion strategy, emphasizing optimization of efficiency and resilience. To determine the optimal configuration of new suppliers, production sites, and warehouses, we conducted a sensitivity analysis across multiple resilience budget levels (β^R). Table 7 details the facilities added at each budget level, illustrating how the network evolves as investment capacity increases.

At lower budgets, the model prioritizes cost-effective enhancements, such as the addition of suppliers. For example, with a 1×10^4 budget, SU CellBoost US TEXAS and SU CellBoost United Kingdom are selected to expand supply capacity and geographic reach. As the budget increases, the model incorporates new warehouses — such as WH USA LEWISBERRY, PENNSYLVANIA and WH Australia PERTH — to reduce transport costs and enhance service coverage.

The framework also evaluates trade-offs between reinforcing existing infrastructure and entering new regions. At a 5×10^6 budget, the selection of MU Brazil and WH Brazil VINHEDO reflects strategic expansion into South America. At higher investment levels (e.g., 1×10^8), the model recommends broader diversification, including facilities such as MU Germany PACKAGING, MU India, and MU Egypt, optimizing for both cost efficiency and resilience under heterogeneous threat scenarios.

Table 7
Newly included facilities in the design, by β^R, with $\beta^D = 0$.

New facility	0	1×10^4	2×10^4	5×10^6	1×10^7	2×10^7	5×10^7	1×10^8	2×10^8
SU CellBoost US TEXAS		✓	✓					✓	
SU CellBoost United Kingdom			✓					✓	✓
WH USA LEWISBERRY, PENNSYLVANIA				✓	✓	✓		✓	✓
WH Australia PERTH					✓	✓		✓	
WH Canada CALGARY						✓			✓
WH Germany KARLSRUHE						✓			
MU Brazil							✓	✓	✓
MU Germany PACKAGING								✓	✓
WH Brazil VINHEDO								✓	✓
SU CellBoost Singapore									✓
MU India									✓
MU Egypt									✓

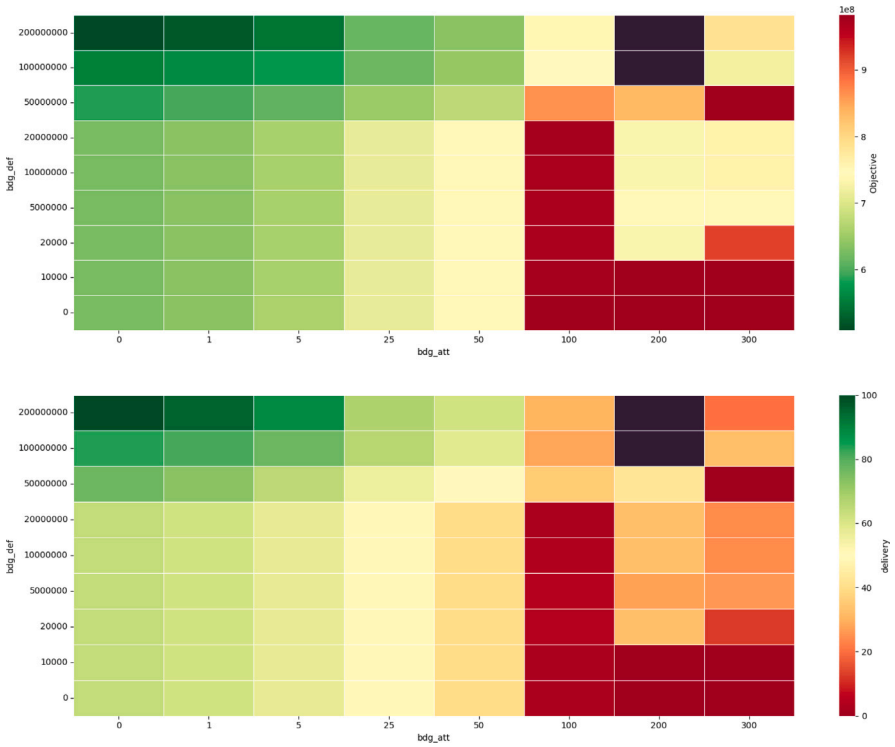

Fig. 10. Resilience grids of β^D and β^R versus objective value and demand delivered [%].

To explore the interaction between resilience and disruption pressures, we conducted a grid-based sensitivity analysis by jointly varying the resilience budget (β^R) and disruption budget (β^D). The resulting resilience grids (Fig. 10) quantify system performance in terms of delivery reliability and operational cost across different budget combinations.

These grids indicate that higher resilience investment enhances disruption absorption through strategies such as multi-sourcing, capacity scaling, and flow rerouting. These adaptive mechanisms sustain service levels and control cost volatility, even under elevated stress conditions.

The analysis further shows that investment levels between 1×10^6 and 2×10^7 provide the most balanced trade-off—delivering robust performance under moderate disruption scenarios ($\beta^D \leq 50$) while avoiding diminishing returns. Under severe disruptions ($\beta^D > 100$), marginal gains decline, reinforcing the value of targeted, efficiency-driven allocation.

Findings and discussion

The computational results provide clear insights into supply chain resilience under climate-related disruptions. Vulnerabilities are concentrated in structurally central facilities — most notably the packaging units in Belgium and the United States —

which lack redundancy and serve as critical hubs in material flows. These nodes are consistently prioritized as disruption targets across scenarios, suggesting that topological centrality, rather than geographic exposure, is the dominant determinant of systemic vulnerability.

By contrast, facility selection in the final network design exhibits greater dispersion. As resilience budgets expand, the model favors diversification not through uniform expansion but via targeted, high-leverage interventions. These include warehouse expansions, selective supplier inclusion, and strategic geographic entry into regions such as Brazil, India, and Egypt. This pattern reflects the model's emphasis on cost-efficient flexibility and redundancy under constrained investment.

A central finding from the climate-adjusted disruption modeling is that while location-specific climate risk shapes relative disruption costs, it does not materially alter which nodes are identified as structurally critical. Disruption and inclusion frequencies align more closely with network topology than with climate risk scores. This does not diminish the role of climate factors. Rather, in the current configuration, central facilities happen to reside in moderately exposed regions. In scenarios where climate exposure and structural centrality coincide, climate-adjusted costs would likely exert greater influence. Thus, climate risk functions as a secondary modifier, amplifying or moderating vulnerability in interaction with network structure.

Finally, sensitivity analysis across budget levels reveals that moderate resilience investments — particularly in the range of 10^6 to 2×10^7 — generate the highest marginal gains in delivery performance and cost efficiency. Beyond this range, returns diminish, especially under high-disruption conditions. This inflection point underscores the strategic value of calibrated investment, enabling firms to balance robustness with financial discipline in resilience planning.

6. Conclusion

This paper introduced a tri-level optimization framework designed to enhance supply chain resilience by adaptively addressing evolving network vulnerabilities. By incorporating both production chain and network flexibility, the model provides strategic guidance for targeted reinforcement and recovery. Computational results showed that increasing flexibility improves resilience significantly, especially when larger design budgets are available. Applying the framework to a pharmaceutical supply chain illustrated its practical value in mitigating climate risks and sustaining operations.

The proposed tri-level optimization framework explicitly models adversarial disruptions, supports adaptive transformation strategies, and integrates fortification with operational flexibility. This structure facilitates anticipatory resilience planning under deep uncertainty by aligning reinforcement and transformation decisions with system-wide vulnerabilities before disruption realization. However, the formulation assumes centralized decision-making under full information and clearly articulated resilience priorities. While this offers a tractable and coordinated foundation for optimization, it abstracts from the decentralized and often conflicting nature of real-world supply chain governance. In practice, supply chains involve multiple stakeholders with divergent goals—ranging from asset prioritization and budget allocation to disruption perception. To address this gap, model outputs could be embedded within a multi-criteria decision-making (MCDM) framework that incorporates stakeholder preferences, enabling adaptation to complex, real-world decision environments.

From a managerial perspective, the findings suggest that resilience investments should target structurally central and hard-to-substitute facilities—particularly core production and packaging nodes. Diversification through multi-sourcing and flexible warehousing yields higher returns than uniform capacity expansion, especially under constrained budgets. Scenario-based stress testing, as enabled by our model, offers a proactive tool for uncovering latent vulnerabilities and guiding strategic resource allocation.

While the model captures complex disruption-defense interactions, it currently assumes deterministic input data and a single-period planning horizon. Extending the framework to incorporate demand uncertainty and time-dependent disruptions would broaden its applicability. Future research could also integrate recovery logistics and examine organizational dimensions of resilience investment—such as decentralized governance, competing objectives, and adaptive learning in uncertain environments.

Future research could expand the disruption model by introducing a multi-component budget to address a range of disruption severities, from minor to catastrophic. This refinement would allow the framework to prioritize adaptive resilience strategies that remain effective across diverse disruption scenarios.

CRediT authorship contribution statement

Maurice Hart Nibbrig: Writing – original draft, Validation, Software, Methodology, Formal analysis, Data curation, Conceptualization. **Shadi Sharif Azadeh:** Writing – review & editing, Validation, Supervision, Methodology, Conceptualization. **M.Y. Maknoon:** Writing – review & editing, Writing – original draft, Validation, Supervision, Methodology, Formal analysis, Conceptualization.

Declaration of competing interest

The authors, Maurice Hart Nibbrig, Sh. Sharif Azadeh, and M.Y. Maknoon, declare that they have no known competing financial interests or personal relationships that could have appeared to influence the work reported in this paper.

This research was conducted independently and received no external funding or support from organizations with a stake in its outcomes.

Data availability

The data that support the findings of this study are available from the corresponding author.

Declaration of Generative AI and AI-assisted technologies in the writing process

During the preparation of this work, the authors used Grammarly to enhance the flow, style, and language of the manuscript. All usage was performed under human oversight, and the authors carefully reviewed and edited the content to ensure its accuracy and integrity. The authors take full responsibility for the final content of the publication.

References

Adenso-Díaz, B., Mar-Ortiz, J., Lozano, S., 2018. Assessing supply chain robustness to links failure. Int. J. Prod. Res. 56 (15), 5104–5117.

Alderson, D.L., Brown, G.G., Carlyle, W.M., Wood, R.K., 2011. Solving defender-attacker-defender models for infrastructure defense. Cent. Infrastruct. Déf. Oper. Res. Dep. Nav. Postgrad. Sch. http://dx.doi.org/10.1287/ics.2011.0047.

Aldrighetti, R., Battini, D., Ivanov, D., 2023. Efficient resilience portfolio design in the supply chain with consideration of preparedness and recovery investments. Omega 117, 102841.

Alikhani, R., Ranjbar, A., Jamali, A., Torabi, S.A., Zobel, C.W., 2023. Towards increasing synergistic effects of resilience strategies in supply chain network design. Omega 116, 102819.

Blackhurst, J., Dunn, K.S., Craighead, C.W., 2011. An empirically derived framework of global supply resiliency. J. Bus. Logist. 32 (4), 374–391.

Bode, C., Wagner, S.M., 2015. Structural drivers of upstream supply chain complexity and the frequency of supply chain disruptions. J. Oper. Manage. 36, 215–228.

Boone, C.A., Craighead, C.W., Hanna, J.B., Nair, A., 2013. Implementation of a system approach for enhanced supply chain continuity and resiliency: A longitudinal study. J. Bus. Logist. 34 (3), 222–235.

Brandon-Jones, E., Squire, B., Van Rossenberg, Y.G., 2015. The impact of supply base complexity on disruptions and performance: the moderating effects of slack and visibility. Int. J. Prod. Res. 53 (22), 6903–6918.

Brusset, X., Teller, C., 2017. Supply chain capabilities, risks, and resilience. Int. J. Prod. Econ. 184, 59–68.

Burgos, D., Ivanov, D., 2021. Food retail supply chain resilience and the COVID-19 pandemic: A digital twin-based impact analysis and improvement directions. Transp. Res. Part E: Logist. Transp. Rev. 152, 102412.

Cardoso, S.R., Barbosa-Póvoa, A.P., Relvas, S., Novais, A.Q., 2015. Resilience metrics in the assessment of complex supply-chains performance operating under demand uncertainty. Omega 56, 53–73.

Carvalho, H., Barroso, A.P., Machado, V.H., Azevedo, S., Cruz-Machado, V., 2012. Supply chain redesign for resilience using simulation. Comput. Ind. Eng. 62 (1), 329–341.

Dempe, S., Zemkoho, A. (Eds.), 2020. Bilevel optimization: Advances and next challenges. Springer Optimization and Its Applications, vol. 161, Springer, Cham.

Dixit, V., Verma, P., Tiwari, M.K., 2020. Assessment of pre and post-disaster supply chain resilience based on network structural parameters with CVaR as a risk measure. Int. J. Prod. Econ. 227, 107655.

Dolgui, A., Ivanov, D., Sokolov, B., 2018. Ripple effect in the supply chain: an analysis and recent literature. Int. J. Prod. Res. 56 (1–2), 414–430.

Forster, P., Storelvmo, T., Alterskjæ, K., et al., 2021. IPCC sixth assessment report (AR6) working group 1: the physical science basis, chap. 7.

Gao, S.Y., Simchi-Levi, D., Teo, C.P., Yan, Z., 2019. Disruption risk mitigation in supply chains: The risk exposure index revisited. Oper. Res. 67 (3), 831–852.

Ghorbani-Renani, N., González, A.D., Barker, K., 2021. A decomposition approach for solving tri-level defender-attacker-defender problems. Comput. Ind. Eng. 153, 107085.

Goldbeck, N., Angeloudis, P., Ochieng, W., 2020. Optimal supply chain resilience with consideration of failure propagation and repair logistics. Transp. Res. Part E: Logist. Transp. Rev. 133, 101830.

Han, J., Shin, K., 2016. Evaluation mechanism for structural robustness of supply chain considering disruption propagation. Int. J. Prod. Res. 54 (1), 135–151.

Hasani, A., Khosrojerdi, A., 2016. Robust global supply chain network design under disruption and uncertainty considering resilience strategies: A parallel memetic algorithm for a real-life case study. Transp. Res. Part E: Logist. Transp. Rev. 87, 20–52.

Hearnshaw, E.J., Wilson, M.M., 2013. A complex network approach to supply chain network theory. Int. J. Oper. Prod. Manage. 33 (4), 442–469.

Hosseini, S., Ivanov, D., 2022. A new resilience measure for supply networks with the ripple effect considerations: A Bayesian network approach. Ann. Oper. Res. 319 (1), 581–607.

Hosseini, S., Ivanov, D., Dolgui, A., 2019. Review of quantitative methods for supply chain resilience analysis. Transp. Res. Part E: Logist. Transp. Rev. 125, 285–307.

Ishfaq, R., 2012. Resilience through flexibility in transportation operations. Int. J. Logist. Res. Appl. 15 (4), 215–229.

Ivanov, D., Dolgui, A., Sokolov, B., Ivanova, M., 2017. Literature review on disruption recovery in the supply chain. Int. J. Prod. Res. 55 (20), 6158–6174.

Ivanov, D., Sokolov, B., Dolgui, A., 2014. The Ripple effect in supply chains: trade-off 'efficiency-flexibility-resilience'in disruption management. Int. J. Prod. Res. 52 (7), 2154–2172.

Johnson, N., Elliott, D., Drake, P., 2013. Exploring the role of social capital in facilitating supply chain resilience. Supply Chain Manag.: An Int. J. 18 (3), 324–336.

Kamalahmadi, M., Parast, M.M., 2016. A review of the literature on the principles of enterprise and supply chain resilience: Major findings and directions for future research. Int. J. Prod. Econ. 171, 116–133.

Kim, Y., Chen, Y.S., Linderman, K., 2015. Supply network disruption and resilience: A network structural perspective. J. Oper. Manage. 33, 43–59.

Kim, Y., Choi, T.Y., Yan, T., Dooley, K., 2011. Structural investigation of supply networks: A social network analysis approach. J. Oper. Manage. 29 (3), 194–211.

Li, Y., Wang, X., Gong, T., Wang, H., 2023. Breaking out of the pandemic: How can firms match internal competence with external resources to shape operational resilience? J. Oper. Manage. 69 (3), 384–403.

Li, Y., Yuan, Y., 2024. Supply chain disruption recovery strategies for measuring profitability and resilience in supply and demand disruption scenarios. RAIRO-Oper. Res. 58 (1), 591–612.

Liu, M., Ding, Y., Chu, F., Dolgui, A., Zheng, F., 2023. Robust actions for improving supply chain resilience and viability. Omega 123, 102972.

Liu, H., Xu, X., Cheng, T., Yu, Y., 2024. Building resilience or maintaining robustness: Insights from relational view and information processing perspective. Transp. Res. Part E: Logist. Transp. Rev. 188, 103609.

Lücker, F., Seifert, R.W., 2017. Building up resilience in a pharmaceutical supply chain through inventory, dual sourcing and agility capacity. Omega 73, 114–124.

Özçelik, G., Faruk Yılmaz, Ö., Betül Yeni, F., 2021. Robust optimisation for ripple effect on reverse supply chain: an industrial case study. Int. J. Prod. Res. 59 (1), 245–264.

Pavlov, A., Ivanov, D., Dolgui, A., Sokolov, B., 2017. Hybrid fuzzy-probabilistic approach to supply chain resilience assessment. IEEE Trans. Eng. Manage. 65 (2), 303–315.
Pettit, T.J., Croxton, K.L., Fiksel, J., 2013. Ensuring supply chain resilience: development and implementation of an assessment tool. J. Bus. Logist. 34 (1), 46–76.
Raaymann, S., Spinler, S., 2024. Measuring supply chain resilience along the automotive value chain—A comparative research on literature and industry. Transp. Res. Part E: Logist. Transp. Rev. 192, 103792.
Ramani, V., Ghosh, D., Sodhi, M.S., 2022. Understanding systemic disruption from the Covid-19-induced semiconductor shortage for the auto industry. Omega 113, 102720.
Ribeiro, J.P., Barbosa-Povoa, A., 2018. Supply chain resilience: Definitions and quantitative modelling approaches–A literature review. Comput. Ind. Eng. 115, 109–122.
Roi, H.V., You, S.S., Nguyen, D.A., Kim, H.-S., 2023. Adaptive decision-making strategy for supply chain systems under stochastic disruptions. LogForum 19 (3), 497–514.
Saglam, Y.C., Çankaya, S.Y., Golgeci, I., Sezen, B., Zaim, S., 2022. The role of communication quality, relational commitment, and reciprocity in building supply chain resilience: A social exchange theory perspective. Transp. Res. Part E: Logist. Transp. Rev. 167, 102936.
Sawik, T., 2022. Stochastic optimization of supply chain resilience under ripple effect: A COVID-19 pandemic related study. Omega 109, 102596.
Sawik, B., 2023. Space mission risk, sustainability and supply chain: review, multi-objective optimization model and practical approach. Sustainability 15 (14), 11002.
Sawik, B., 2024. Optimizing last-mile delivery: A multi-criteria approach with automated smart lockers, capillary distribution and crowdshipping. Logistics 8 (2), 52.
Sawik, T., Sawik, B., 2024. Risk-averse decision-making to maintain supply chain viability under propagated disruptions. Int. J. Prod. Res. 62 (8), 2853–2867.
Tang, C.S., 2006. Perspectives in supply chain risk management. Int. J. Prod. Econ. 103 (2), 451–488.
Tiwari, M., Bryde, D.J., Stavropolou, F., Dubey, R., Kumari, S., Foropon, C., 2024. Modelling supply chain visibility, digital technologies, environmental dynamism and healthcare supply chain resilience: An organisation information processing theory perspective. Transp. Res. Part E: Logist. Transp. Rev. 188, 103613.
Tukamuhabwa, B.R., Stevenson, M., Busby, J., Zorzini, M., 2015. Supply chain resilience: definition, review and theoretical foundations for further study. Int. J. Prod. Res. 53 (18), 5592–5623.
Wang, X., Herty, M., Zhao, L., 2016. Contingent rerouting for enhancing supply chain resilience from supplier behavior perspective. Int. Trans. Oper. Res. 23 (4), 775–796.
Wieland, A., Durach, C.F., 2021. Two perspectives on supply chain resilience. J. Bus. Logist. 42 (3), 315–322.
Wieland, A., Wallenburg, C.M., 2013. The influence of relational competencies on supply chain resilience: a relational view. Int. J. Phys. Distrib. Logist. Manage. 43 (4), 300–320.
Yılmaz, Ö.F., Özçelik, G., Yeni, F.B., 2021. Ensuring sustainability in the reverse supply chain in case of the ripple effect: A two-stage stochastic optimization model. J. Clean. Prod. 282, 124548.
Yılmaz, Ö.F., Yeni, F.B., Yılmaz, B.G., Özçelik, G., 2023. An optimization-based methodology equipped with lean tools to strengthen medical supply chain resilience during a pandemic: A case study from Turkey. Transp. Res. Part E: Logist. Transp. Rev. 173, 103089.